SIAM J. SCI. COMPUT.
Vol. 42, No. 5, pp. A2910–A2942

EFFICIENT ALGORITHMS FOR COMPUTING MULTIDIMENSIONAL INTEGRAL FRACTIONAL LAPLACIANS VIA SPHERICAL MEANS*

BOXI XU†, JIN CHENG‡, SHINGYU LEUNG§, AND JIANLIANG QIAN¶

Abstract. We develop efficient algorithms for computing the multidimensional fractional operator $(-\Delta_x)^{\frac{\alpha}{2}}$ in the form of hypersingular integral in the entire space, where the operator is the so-called integral fractional Laplacian when $0 < \alpha < 2$. By introducing polar coordinates, we reduce applying the multidimensional integral fractional operator to a function to applying the resulting one-dimensional fractional operator to the spherical mean of the underlying function. We propose two algorithms to compute spherical means of a given function: one by solving standard wave equations and the other by solving Darboux's equations. We further apply a finite difference numerical quadrature approach to compute the one-dimensional fractional operator. Our methodology is equally applicable to computing the action of the integral fractional Laplacian, the extended integral fractional Laplacian, and the Riesz potential operator, respectively, and the computational complexity for applying each of the three operators is $\mathcal{O}(L^{n+1})$, where L denotes the number of mesh points in each spatial direction and n is the spatial dimension. Numerical examples, including algebraically decaying functions with varying regularities, demonstrate the performance and convergence rates of our new algorithms.

Key words. fractional Laplacian, spherical means, Riesz operator, hypersingular operator, Darboux's equation

AMS subject classifications. 78A05, 78A46, 78M35

DOI. 10.1137/19M1262358

1. Introduction.

The fractional Laplacian is fundamental in modeling phenomena of nonlocal diffusion and long-range interactions, which arises in anomalous diffusion [32, 33, 43] and α-stable Lévy process [5, 31, 46, 39]. Since the fractional Laplacian is nonlocal, it is considerably more difficult to develop an efficient and accurate discretization for such an operator. In this paper, we propose a novel efficient algorithm based on spherical means to discretize the multidimensional (multi-D) integral fractional Laplacian defined by means of a pointwise integral formula over $\mathbb{R}^n$, and our new methodology is also applicable to the extended fractional Laplacian and the Riesz potential operator, the latter of which can be used to solve the fractional Poisson equation.

*Submitted to the journal's Methods and Algorithms for Scientific Computing section May 17, 2019; accepted for publication (in revised form) June 26, 2020; published electronically September 28, 2020.

https://doi.org/10.1137/19M1262358

Funding: The work of the first author was supported by Shanghai Pujiang Program 18PJ1403600. The work of the second author was supported by the Natural Science Foundation of China through grants 11771270 and 11971121. The work of the third author was supported by the Hong Kong RGC through grant 16309316. The work of the fourth author was partially supported by the National Science Foundation.

†School of Mathematics, Shanghai University of Finance and Economics, Shanghai 200433, China (xu.boxi@mail.sufe.edu.cn).

‡School of Mathematical Sciences, Fudan University, Shanghai 200433, China (jcheng@fudan.edu.cn).

§Department of Mathematics, The Hong Kong University of Science and Technology, Clear Water Bay, Hong Kong (masyleung@ust.hk).

¶Department of Mathematics, Michigan State University, East Lansing, MI 48824 (jqian@msu.edu).

The fractional Laplacian $(-\Delta_x)^{\frac{\alpha}{2}}$ in the entire space $\mathbb{R}^n$ can be defined in many equivalent ways, as shown by [29]. We adopt the definition in the form of hypersingular integral,

$$(-\Delta_x)^{\frac{\alpha}{2}} f(x) := C_{n,\alpha}\ \text{p.v.} \int_{\mathbb{R}^n} \frac{f(x)-f(y)}{|x-y|^{n+\alpha}}\,\mathrm{d}y, \quad x \in \mathbb{R}^n, \tag{1.1}$$

where f is a sufficiently smooth function which may or may not be compactly supported, $C_{n,\alpha}$ is a normalization constant, and $\alpha \in (0,2)$; following [6], we call this operator the integral fractional Laplacian. This integral operator, also known as the Riesz fractional derivative operator, epitomizes two essential features of fractional integral operators, singularity and nonlocality, which give rise to major difficulties in analysis and discretization.

Letting Ω be a bounded Lipschitz domain in $\mathbb{R}^n$, we consider the so-called extended Dirichlet problem defined by the fractional powers of the Laplace operator. For $u : \Omega \to \mathbb{R}$, we first extend u by zero outside Ω and next use definition (1.1) of the integral fractional Laplacian to formulate the following extended Dirichlet problem so as to find $\widetilde{u}$:

$$(-\Delta_x)^{\frac{\alpha}{2}} \widetilde{u} = g \quad \text{in } \Omega, \qquad \widetilde{u} = 0 \quad \text{in } \Omega^c = \mathbb{R}^n \backslash \Omega, \tag{1.2}$$

where $g : \Omega \to \mathbb{R}$ is a given function in a suitable space and $\widetilde{w}$ is the extension by zero to $\mathbb{R}^n$ of a function $w : \Omega \to \mathbb{R}$.

To treat the singularity of the integral fractional Laplacian in the extended Dirichlet problem (1.2), a discretization scheme by subtracting singularity is proposed in [37] without introducing appropriate windowing functions, and the work in [34] has carefully discussed and computationally illustrated the importance and accuracy of such windowing for singularity subtraction. In this case, since $u \equiv 0$ in $\mathbb{R}^n \backslash \Omega$ and the Lipschitz domain Ω is bounded, the work in [34] does not need to deal with the issue of nonlocality, namely, the asymptotic behavior of the tail of the underlying function u at infinity in evaluating the fractional Laplacian; consequently, the windowing finite difference approach for subtracting singularity has been successfully applied to the multi-D homogeneous extended Dirichlet problems as well.

Due to the nonlocality of the fractional Laplacian, the above windowing-based methods can only deal with compactly supported functions or rapidly decaying functions. Realizing the lack of numerical analysis for a diversity of numerical methods for fractional Laplacians, the works in [23, 24] have proposed and analyzed finite difference-quadrature approaches for discretizing the one-dimensional (1-D) integral fractional Laplacian. These approaches first split the hypersingular integral into two parts, the singular part and the regular part, over $\mathbb{R}^1$. For the singular part, assuming that the underlying function f has enough regularity, these methods are able to symmetrize the hypersingular integral to obtain a regular integral, and these methods further apply high-order Taylor expansions to develop a fully discrete approximation of the singular part; however, this discrete scheme has an undesirable feature: Its convergence order is not uniform with respect to α and deteriorates as the fractional order α goes to 2, which is inconsistent with that of the central-difference approximation of the classical Laplacian. For the regular part, which is an integral over an unbounded interval, the works in [23, 24] first developed infinite-sum finite difference-quadrature formulas with positive weights for the integral over the unbounded interval, and then the method truncates the infinite sum into a finite sum, which effectively truncates the unbounded interval to a bounded one. Moreover, the works in [23, 24] have developed an ingenious approach to treat the truncated boundary terms (the tail of

the fractional operator) by analyzing the asymptotic behavior of the underlying function f when the function has only algebraic decaying in the far field, and this tail treatment is crucial for an accurate evaluation of the fractional Laplacian. Although the deteriorating convergence rate of the 1-D discrete approximation [23, 24] when α going to 2 can be remedied by applying weighted trapezoidal rules to the weighted integral of a weak singular function as shown in [16], the 1-D tail treatment cannot be easily extended to multi-D cases. See [45, 19, 3, 34] for more on discretizing 1-D integral fractional Laplacians.

Because most of the above cited works are not able to compute accurately the action of a multi-D integral fractional Laplacian to a function f defined in the entire space $\mathbb{R}^n$ with a tail decaying to zero algebraically, we propose a novel, efficient, and accurate numerical method on a uniform mesh to achieve exactly such a purpose. Since the kernel of the integral fractional Laplacian in the form of hypersingular integral is a radial function, we are able to apply a polar-coordinate transformation to reduce the action of the multi-D integral fractional operator to that of a 1-D fractional operator to the spherical means of the underlying function, where the spherical mean of a function plays an important role in the sense that it reduces the multi-D singularity and nonlocality to the 1-D ones. In fact, introducing spherical means into the multi-D integral fractional Laplacian enables us to reduce the multi-D fractional integral to a corresponding 1-D fractional integral, which is much easier to evaluate. Since the spherical mean of a function satisfies Darboux's equation, which is a wave-like equation, we can develop efficient algorithms to solve this equation. By carefully balancing numerical errors arising from different sources, we obtain high-order accurate schemes for computing the fractional Laplacian efficiently. Since, in our formulation, the computational domain is $\Omega \times [0, R_0]$ with R_0 the largest radius of the spheres on which spherical means are to be computed, the dimension of the computational domain is $n + 1$. Letting L be the number of mesh points in each direction, the total number of mesh points of our algorithm is $\mathcal{O}(L^{n+1})$, and accordingly the computational complexity of applying the integral fractional Laplacian is proportional to $\mathcal{O}(L^{n+1})$. The methodology can be equally applied to evaluate multi-D extended fractional Laplacians and Riesz potential operators, the latter of which solve the fractional Poisson equation.

Other related work. Since there are many equivalent definitions of the fractional Laplacian in the entire space $\mathbb{R}^n$, many different discretizations of the operator have been introduced from different perspectives based on different formulations. One prominent feature of these different discretizations is that they usually do not coincide when restricted to problems posed on bounded domains. To illustrate these subtle points, following [6] we consider the following problem with vanishing Dirichlet boundary conditions,

$$(-\Delta_x)^{\frac{\alpha}{2}} u = g \quad \text{in } \Omega, \qquad u\Big|_{\partial\Omega} = 0, \tag{1.3}$$

where α, g, and Ω are defined as in problem (1.2).

According to [6], we may apply the spectral definition of the fractional Laplacian [35, 42, 10, 47] to discretize problem (1.3). However, the solution defined by the integral fractional Laplacian (1.1) via solving the extended Dirichlet problem (1.2) is *different* from that defined by the spectral fractional Laplacian via solving the Caffarelli–Silvestre [9] extension problem in a bounded domain [6]. In order to handle the non-integrable kernel in the integral fractional Laplacian (1.2), the Caffarelli–Silvestre [9] extension allows us to convert problem (1.3) for $\Omega = \mathbb{R}^n$ into a Dirichlet-to-Neumann

map problem in an extended space $\mathbb{R}^n \times (0, \infty)$, where the solution of the problem (1.3) can be read off from the trace of the solution of the extension problem in the cylinder $\mathbb{R}^n \times (0, \infty)$; see [38] for general references. Furthermore, the works in [8, 44] have shown that a similar Caffarelli–Silvestre extension is valid for the spectral fractional Laplacian in a bounded domain Ω provided that a vanishing Dirichlet condition is imposed on the lateral boundary $\partial\Omega \times (0, \infty)$. Based on the spectral definition in [8, 44], the works in [11, 36] have developed finite-element methods to discretize the spectral fractional Laplacian and solve the corresponding Dirichlet problem, where the total number of degrees of freedom of these methods amounts to $\mathcal{O}(L^{n+1})$ with L the number of graded mesh points in the truncated extended direction; in addition, based on [11, 36], the work in [12] has developed a multilevel method with computational complexity proportional to $\mathcal{O}(L^{n+1})$ for solving the resulting linear system. A recent work in [13] developed an efficient and accurate numerical method for the spectral fractional Laplacian equation by using the matrix diagonalization method to reduce the $n + 1$-dimensional problem to a sequence of n-dimensional Poisson-type equations and resolving the singularity by applying the enriched spectral method in the extended dimension. See [6, 21, 22] for other related works along this line.

The extended Dirichlet problem (1.2) defined by the integral fractional Laplacian can be also solved by finite element methods [1, 2]; in this case, the nonlocality of the integral fractional Laplacian implies that it depends on data prescribed everywhere outside Ω, and the vanishing, extended Dirichlet boundary conditions should be prescribed; see [15, 18, 38, 30] for more.

The solution to (1.3) defined by either the integral or the spectral fractional Laplacian can be represented using Dunford–Taylor integrals [7], and the resulting integrals can be further discretized by using finite-element methods and sinc quadratures [7, 6]; see [6] and references therein for more details.

Although our proposed algorithms are of computational complexity $O(L^{n+1})$, our methods are equally applicable to computing the action of the multi-D integral fractional Laplacian, the multi-D extended integral fractional Laplacian, and the multi-D Riesz potential operator, respectively, to functions defined in the entire space with tails decaying to zero algebraically, while existing methods with better computational complexity [34, 4] are mostly restricted to handle problems with data defined in bounded domains rather than in the entire space. Therefore, in comparison to [34, 4], our proposed method is unique in the sense that it can handle functions defined in the entire space with tails decaying to zero algebraically, and we should understand our algorithm to be efficient precisely because of this unique aspect.

The paper is structured as follows. In section 2, we first recall definitions of the fractional Laplacian operator and the Riesz potential operator, and we also introduce a definition of the extended fractional Laplacian for large α. In the following sections, these Riesz derivative/integral operators are discretized and implemented numerically. In section 3, the relations between any n-dimensional operator and the corresponding 1-D operator are derived using spherical means, and we also develop two approaches to generate the spherical mean of a given function. Moreover, the asymptotic behavior of the tail of the spherical mean are estimated, which leads to an appropriate truncation of the computational domain. In section 4, we summarize our numerical method first and detail our numerical schemes for each step of the method. Sections 5–7 show various numerical examples to demonstrate the performance and convergence rates of our new algorithm.

2. Fractional Laplacian and Riesz potential operators: Some facts. We recall the definition of the integral fractional Laplacian operator in the entire space $\mathbb{R}^n$ in the form of a hypersingular integral, the kernel of which has a singularity at the origin of order greater than n, where n is the dimension of the space. For convenience without confusion, in the following presentation we will simply call the "integral fractional Laplacian" the "fractional Laplacian."

DEFINITION 2.1. *The fractional Laplacian is defined by the following hypersingular integral:*

$$(-\Delta_x)^{\frac{\alpha}{2}} f(x) := C_{n,\alpha} \text{ p.v.} \int_{\mathbb{R}^n} \frac{f(x)-f(y)}{|x-y|^{n+\alpha}} \,\mathrm{d}y, \tag{2.1}$$

where the dimension $n \geqslant 1$, $\alpha \in (0,2)$, f is in a suitable function space, and p.v. *denotes the Cauchy principal value. The constant $C_{n,\alpha}$ takes the following value:*

$$C_{n,\alpha} = -\frac{2^\alpha \Gamma\left(\frac{n+\alpha}{2}\right)}{\pi^{\frac{n}{2}} \Gamma\left(-\frac{\alpha}{2}\right)}, \tag{2.2}$$

where $\Gamma(z)$ is the gamma function.

By using the Fourier transform, we have the following equivalent definition of the fractional Laplacian:

$$\mathcal{F}_x\left[(-\Delta_x)^{\frac{\alpha}{2}} f\right](\xi) = |\xi|^\alpha \mathcal{F}_x[f](\xi), \tag{2.3}$$

where the Fourier transform is defined by

$$\mathcal{F}_x[f](\xi) := (2\pi)^{-\frac{n}{2}} \int_{\mathbb{R}^n} f(x) e^{-\mathbf{i}\,\xi\cdot x} \,\mathrm{d}x. \tag{2.4}$$

Since the Fourier transform of the hypersingular integral (2.1) yields the formula (2.3), the fractional Laplacian operator sometimes is also called the *Riesz derivative operator* (see page 499 of [41]). From a more broad perspective, we consider the Riesz potential operator.

DEFINITION 2.2. *The Riesz potential operator is defined by*

$$R_x^\alpha \varphi(x) = (-\Delta_x)^{-\frac{\alpha}{2}} \varphi(x) := C_{n,\alpha}^R \int_{\mathbb{R}^n} \frac{\varphi(y)}{|x-y|^{n-\alpha}} \,\mathrm{d}y, \tag{2.5}$$

where $\alpha > 0$ and $\alpha \neq n, n+2, n+4, \ldots, \varphi$ is in a suitable function space and the constant $C_{n,\alpha}^R$ is

$$C_{n,\alpha}^R = \frac{2^{-\alpha}\Gamma\left(\frac{n-\alpha}{2}\right)}{\pi^{\frac{n}{2}}\Gamma\left(\frac{\alpha}{2}\right)}. \tag{2.6}$$

When $\alpha \in (0,n)$ and $p \in (1, \frac{n}{\alpha})$, the Riesz potential operator R_x^α is bounded from $L^p(\mathbb{R}^n)$ into $L^{p^*}(\mathbb{R}^n)$ (or the weighted space $L^p(\mathbb{R}^n; |x|^{-\alpha p})$), where $p^* := \frac{np}{n-\alpha p}$ is known as the *Sobolev limiting exponent*. When $\alpha \geqslant n$ and $p \geqslant \frac{n}{\alpha}$, the proof of boundedness of the Riesz potential operator is more involved; in this case, we have to introduce some weighted spaces $L^p(\mathbb{R}^n; |x|^{-\alpha p})$ and Lizorkin spaces $\Phi \subset \mathcal{S}(\mathbb{R}^n)$; see page 39 of [40], page 487 of [41], and the references therein.

As shown on page 512 of [41], the Riesz derivative operator, or the fractional Laplacian operator (2.1), is an inverse operator to the Riesz potential operator (2.5). In fact, for any $\varphi \in L^p(\mathbb{R}^n)$ with $\alpha \in (0, n)$ and $p \in (1, \frac{n}{\alpha})$, letting $f = R_x^\alpha \varphi \in L^{p^*}(\mathbb{R}^n)$ and $f \to 0$ as $|x| \to \infty$, the Riesz derivative operator is the left inverse to the Riesz potential operator,

$$(-\Delta_x)^{\frac{\alpha}{2}} f = (-\Delta_x)^{\frac{\alpha}{2}} R_x^\alpha \varphi = \varphi \in L^p(\mathbb{R}^n) \quad \text{for} \quad f \in L^{p^*}(\mathbb{R}^n). \tag{2.7}$$

Moreover, assuming that $\alpha \in (0, n)$, $\varphi(x)$ belongs to the *Schwartz space* $\mathcal{S}(\mathbb{R}^n)$, $\varphi(x) \geqslant 0$, and $\varphi(x) \geqslant \varphi_0 > 0$ for $|x| < 1$, according to definition (2.5) of the Riesz potential operator, we have that

$$f(x) = R_x^\alpha \varphi(x) \geqslant C_{n,\alpha}^R \int_{|y|<1} \frac{\varphi_0}{|x-y|^{n-\alpha}} \, \mathrm{d}y \geqslant \frac{C}{|x|^{n-\alpha}} \quad \text{as } |x| \to \infty; \tag{2.8}$$

in other words, even if its Riesz derivative belongs to the Schwartz space $\mathcal{S}(\mathbb{R}^n)$, a function f does not necessarily vanish exponentially at infinity.

The parameter α of the fractional Laplacian (2.1) belongs to the interval $(0, 2)$. However, for the case $\alpha \geqslant 2$, we may define an extension of the hypersingular integral (2.1).

DEFINITION 2.3. *For an even order $j = 2, 4, 6, \ldots$ only,*

$$(-\Delta_x)_j^{\frac{\alpha}{2}} f(x) := C_{n,\alpha,j} \text{ p.v.} \int_{\mathbb{R}^n} \frac{\mathcal{D}_j(x, y; f)}{|y|^{n+\alpha}} \, \mathrm{d}y, \quad \alpha \in (0, j), \tag{2.9}$$

where the normalization constant is

$$C_{n,\alpha,j} = (-1)^{\frac{j}{2}} \frac{2^{\alpha-j-1}\Gamma\left(\frac{n+\alpha}{2}\right)}{\pi^{\frac{n-1}{2}}\Gamma\left(\frac{1+\alpha}{2}\right)\int_0^\infty (\sin t)^j t^{-1-\alpha} \, \mathrm{d}t} \tag{2.10}$$

and the jth-order centered difference is defined by

$$\mathcal{D}_j(x, y; f) := \delta_y^j [f](x) = \sum_{k=0}^{j} (-1)^k \binom{j}{k} f\big(x + (\tfrac{j}{2} - k)y\big), \tag{2.11}$$

where $\binom{j}{k}$ is the binomial coefficient.

When $j = 2$, we recover the integral (2.1) from the integral (2.9) since the second-order finite difference is $\mathcal{D}_2(x, y; f) = f(x + y) - 2f(x) + f(x - y)$ and the constant $C_{n,\alpha} = -2C_{n,\alpha,2}$. Consequently, we call the integral (2.9) the *extended fractional Laplacian*, or the *extended Riesz derivative operator*, since it still satisfies the relation (2.3) with the normalization constant $C_{n,\alpha,j}$. Furthermore, when $\alpha \in (0, n)$, the extended Riesz derivative operator (2.9) is also the left inverse to the Riesz potential operator (2.5).

In addition, when $\alpha \geqslant n$, we assume that $\mathcal{D}_j(\cdot, y; f) \in L^p(\mathbb{R}^n)$ for any $y \in \mathbb{R}^n$ so that the integral (2.9) is well defined; see page 532 of [41] for details.

3. Dimensional reduction for fractional operators. Based on spherical means, we will derive some formulas which reduce any n-dimensional fractional Laplacian to a 1-D operator on the entire real axis $\mathbb{R}^1$ or on the half-axis $(0, \infty)$, and these formulas can be numerically evaluated easily.

3.1. Spherical mean–based dimensional reduction. We start from the spherical mean $\mathcal{U}(x,r;f)$ of a continuous function f,

$$\mathcal{U}(x,r;f) := \frac{1}{\omega_n}\int_{\mathbb{S}^{n-1}} f(x+r\omega)\,\mathrm{d}\omega, \tag{3.1}$$

where the surface area ω_n of $\mathbb{S}^{n-1}$ is

$$\omega_n := \int_{\mathbb{S}^{n-1}} \mathrm{d}\omega = \frac{2\pi^{\frac{n}{2}}}{\Gamma\left(\frac{n}{2}\right)}. \tag{3.2}$$

Then we obtain the following Theorem 3.1 based on the definition (2.1) of the fractional Laplacian, where the notation $\left(-\partial_r^2\right)^{\frac{\alpha}{2}}$ denotes the 1-D fractional Laplacian with respect to the variable $r\in\mathbb{R}^1$.

THEOREM 3.1. *Let f be sufficiently smooth. Then*

$$(-\Delta_x)^{\frac{\alpha}{2}} f(x) = d_{n,\alpha}\left[\left(-\partial_r^2\right)^{\frac{\alpha}{2}}\mathcal{U}(x,r;f)\right]\Big|_{r=0}, \tag{3.3}$$

where $d_{n,\alpha} = \frac{\omega_n C_{n,\alpha}}{2C_{1,\alpha}}$.

Proof. According to the definition (2.1), we carry out a polar-coordinate change to obtain

$$\begin{aligned}
(-\Delta_x)^{\frac{\alpha}{2}} f(x) &= C_{n,\alpha}\ \text{p.v.}\int_{\mathbb{R}^n}(f(x)-f(y))\,|x-y|^{-n-\alpha}\,\mathrm{d}y\\
&= C_{n,\alpha}\ \text{p.v.}\int_{\mathbb{R}^n}(f(x)-f(x-y))\,|y|^{-n-\alpha}\,\mathrm{d}y\\
&= C_{n,\alpha}\ \text{p.v.}\int_0^\infty\int_{\mathbb{S}^{n-1}}(f(x)-f(x-\rho\omega))\,\rho^{-n-\alpha}\rho^{n-1}\,\mathrm{d}\omega\,\mathrm{d}\rho \qquad (3.4a)\\
&= \frac{C_{n,\alpha}}{2}\ \text{p.v.}\int_{\mathbb{R}^1}\left(\int_{\mathbb{S}^{n-1}} f(x)\mathrm{d}\omega - \int_{\mathbb{S}^{n-1}} f(x-\rho\omega)\mathrm{d}\omega\right)|\rho|^{-1-\alpha}\,\mathrm{d}\rho\\
&= \frac{\omega_n C_{n,\alpha}}{2}\ \text{p.v.}\int_{\mathbb{R}^1}(\mathcal{U}(x,0;f)-\mathcal{U}(x,-\rho;f))\,|\rho|^{-1-\alpha}\,\mathrm{d}\rho\\
&= \frac{\omega_n C_{n,\alpha}}{2C_{1,\alpha}}\left[\left(-\partial_r^2\right)^{\frac{\alpha}{2}}\mathcal{U}(x,r;f)\right]\Big|_{r=0}, \qquad (3.4b)
\end{aligned}$$

where the Cauchy principal values (p.v.) depend on the singularities of each integrand. ∎

Similarly, for the extended fractional Laplacian (2.9) and the Riesz potential operator (2.5), we have the following results since the kernel of each integral has radial symmetry: $|x|^{-n-\alpha}$ or $|x|^{-n+\alpha}$, where the notations $\left(-\partial_r^2\right)_j^{\frac{\alpha}{2}}$ and R_r^α denote the corresponding 1-D operator with respect to $r\in\mathbb{R}^1$, respectively.

THEOREM 3.2. *Let f and φ be sufficiently smooth functions. Then*

$$(-\Delta_x)_j^{\frac{\alpha}{2}} f(x) = d_{n,\alpha,j}\left[\left(-\partial_r^2\right)_j^{\frac{\alpha}{2}}\mathcal{U}(x,r;f)\right]\Big|_{r=0}, \tag{3.5a}$$

$$R_x^\alpha\varphi(x) = d_{n,\alpha}^R\left[R_r^\alpha\mathcal{U}(x,r;\varphi)\right]\Big|_{r=0}, \tag{3.5b}$$

where $d_{n,\alpha,j} = \frac{\omega_n C_{n,\alpha,j}}{2C_{1,\alpha,j}}$ and $d_{n,\alpha}^R = \frac{\omega_n C_{n,\alpha}^R}{2C_{1,\alpha}^R}$.

In summary, the above two theorems reduce any n-dimensional Riesz derivative operator or fractional integral operator to a 1-D operator of the same type. Taking Theorem 3.1, for example, the right-hand side of the formula (3.3) is the 1-D fractional Laplacian $\left(-\partial_r^2\right)^{\frac{\alpha}{2}}$ acting on the function $\mathcal{U}(x,r;f)$ instead of f and only evaluated at the origin $r=0$. Therefore, we just need to evaluate the 1-D fractional Laplacian on the entire r-axis numerically.

However, since the spherical mean function $\mathcal{U}(x,r;f)$ is even with respect to the variable r, we can also restrict our formulations to the half-axis $r\in(0,\infty)$.

COROLLARY 3.1. *Denote the operator* $[U_r f](x) := \mathcal{U}(x,r;f)$. *When* $\alpha\in(0,2)$, *the fractional Laplacian* (2.1) *is represented as*

$$(-\Delta_x)^{\frac{\alpha}{2}} f(x) = \omega_n C_{n,\alpha}\ \text{p.v.}\int_0^\infty \frac{[(I-U_r)\,f](x)}{r^{1+\alpha}}\,\mathrm{d}r, \tag{3.6}$$

where I *is the identity operator and the* p.v. *depends on the singularity at* $r=0$.

Proof. The proof is based on (3.4a) in Theorem 3.1. ∎

COROLLARY 3.2. *The extended fractional Laplacian* (2.9) *with* $\alpha\in(0,j)$ *and the Riesz potential* (2.5) *with* $\alpha>0$, $\alpha\neq n,n+2,\dots$ *are represented as, respectively,*

$$(-\Delta_x)_j^{\frac{\alpha}{2}} f(x) = \omega_n C_{n,\alpha,j}\ \text{p.v.}\int_0^\infty \frac{[\mathcal{D}_j(0,r;U_r)f](x)}{r^{1+\alpha}}\,\mathrm{d}r, \tag{3.7a}$$

$$R_x^\alpha\varphi(x) = \omega_n C_{n,\alpha}^R\ \text{p.v.}\int_0^\infty \frac{[U_r\varphi](x)}{r^{1-\alpha}}\,\mathrm{d}r. \tag{3.7b}$$

According to [41], the above representation (3.6) or (3.7a) of the n-dimensional fractional Laplacian (2.1) or (2.9) is called the 1-D *Marchaud-type fractional derivative* of the function $U_r f$, while the integral (3.7b) corresponding to the Riesz potential operator (2.5) is called the 1-D *Liouville-type fractional integral* of the function $U_r\varphi$.

Since the exponent of the operator $(I-U_r)$ is one in formula (3.6) in Corollary 3.1, we may use this formula to numerically compute the fractional Laplacian. The corresponding formulas of the extended fractional Laplacian (2.9) and (3.7a) can also be used in computation since the following expression holds:

$$[\mathcal{D}_j(0,r;U_r)f](x) = \sum_{k=0}^{j}(-1)^k\binom{j}{k}[U_{(\frac{j}{2}-k)r}f](x) = \sum_{k=0}^{j}(-1)^k\binom{j}{k}\mathcal{U}\big(x,(\frac{j}{2}-k)r;f\big). \tag{3.8}$$

Thus, in all cases mentioned above, we only need to implement the 1-D Marchaud-type fractional derivatives (3.6) and (3.7a) or the 1-D Liouville-type fractional integral (3.7b) on the half-axis $(0,\infty)$ numerically.

Instead of using the original definitions, we may use formulas (3.3), (3.5), (3.6), and (3.7) to compute the n-dimensional fractional operators. In other words, once the spherical mean $\mathcal{U}(x,r;f)$ of a function f is generated, we can utilize a suitable 1-D operator to act on the spherical mean to produce the effect of n-dimensional fractional operators. Thus, in the next subsection, we look into how to generate spherical means of a given function.

3.2. Constructing spherical means. Since the spherical mean function plays an important role in our method, we will introduce some properties of this function first, and we will further propose several suitable ways to generate spherical means of any function.

As shown by the definition (3.1), the spherical mean $\mathcal{U}(x,r;f)$ represents the average of the function f over a sphere of radius r centered at the point x. Thus, for the spherical mean $\mathcal{U}(x,r;f)$, we have the following results.

LEMMA 3.1. (1) *The spherical mean of a function f is an even function of the variable r, that is,*

$$\mathcal{U}(x,r;f) = \mathcal{U}(x,-r;f). \tag{3.9}$$

(2) *If the function f is continuous, then the spherical mean $\mathcal{U}(x,r;f)$ is continuous in both x and r, and it satisfies*

$$\mathcal{U}(x,0;f) = f(x). \tag{3.10}$$

It is also known that the spherical mean $\mathcal{U}(x,r;f)$ satisfies the following initial value problem of *Darboux's differential equation*, which contains a term with removable singularity at the origin:

$$\begin{cases} \partial_r^2 u(x,r) + \dfrac{n-1}{r}\partial_r u(x,r) = \Delta_x u(x,r), & r > 0,\ x \in \mathbb{R}^n, \\ u(x,0) = f(x), & x \in \mathbb{R}^n, \\ \partial_r u(x,0) = 0, & x \in \mathbb{R}^n. \end{cases} \tag{3.11}$$

LEMMA 3.2 (Courant and Hilbert [14], page 699). *The spherical mean $\mathcal{U}(x,r;f) = u(x,r)$ of function f is determined uniquely by the solution of the initial value problem* (3.11). *Furthermore, defining $u(x,r) = u(x,-r)$ for $r < 0$, the solution $u(x,r)$ of Darboux's differential equation* (3.11) *can be uniquely continued to negative r as a continuously differentiable function, and it is an even function of r.*

REMARK 3.1. We mention in passing that the spherical mean of a function f is C^1 so that it has enough regularity at $r = 0$ according to the above lemma. Moreover, for compactly supported functions on rectangular domains, fast Fourier transform–based spectral methods can be quite efficient in generating corresponding spherical means. However, in this work, we are interested in computing spherical means for generic functions of algebraically decaying tails.

REMARK 3.2. On the one hand, since our spherical mean–based multi-D integral fractional Laplacian reduces the action of a multi-D integral fractional Laplacian to that of a 1-D fractional Laplacian to the underlying spherical mean function, all essential difficulties of multi-D fractional Laplacians are shown in terms of difficulties of applying the 1-D fractional Laplacian to a spherical mean function at the origin. On the other hand, since the Caffarelli–Silvestre extension [9] reformulates the nonlocal integral fractional Laplacian in the entire ambient space into a local PDE problem in the extended space, all essential difficulties of the integral fractional Laplacian are shown in terms of difficulties of computing the Dirichlet-to-Neumann map in the extended space. Therefore, although the viewpoint of the Caffarelli–Silvestre extension is dramatic in that it changes a nonlocal problem in the ambient space to a local problem in the extended space, our formulation of the multi-D integral fractional Laplacian allows us to take advantage of existing numerical methods for 1-D integral fractional Laplacians to develop effective algorithms for multi-D operators, including not only multi-D integral fractional Laplacians but also multi-D Riesz potential operators.

3.2.1. Decomposition of spherical means into wave solutions. In fact, there is a one-to-one correspondence between the solution of the standard wave equation and that of Darboux's differential equation.

On the one hand, the solution $w(x,t)$ of the following standard wave equation can be represented by the spherical mean $\mathcal{U}(x,r;f)$ of function f:

$$\begin{cases} \partial_t^2 w(x,t) = \Delta_x w(x,t), & t>0,\ x\in\mathbb{R}^n,\\ w(x,0) = g_1(x), & x\in\mathbb{R}^n,\\ \partial_t w(x,0) = g_2(x), & x\in\mathbb{R}^n. \end{cases} \tag{3.12}$$

Here, we use the notation $\mathcal{W}(x,t;\{g_1,g_2\}) = w(x,t)$ to emphasize the dependence on the initial data $\{g_1,g_2\}$ of the corresponding solution of the standard wave equation.

LEMMA 3.3 (Courant and Hilbert [14], page 682). *Assume that the function f is smooth enough. Then $\mathcal{W}(x,t;\{f,0\}) = \mathcal{U}(x,t;f)$ for $n=1$, and the following classical formula holds for any $n \geqslant 2$:*

$$\mathcal{W}(x,t;\{f,0\}) = \frac{1}{\Gamma(n-1)}(\partial_t)^{n-1}\int_0^t r\left(t^2-r^2\right)^{\frac{n-3}{2}}\mathcal{U}(x,r;f)\,\mathrm{d}r. \tag{3.13}$$

The above formula (3.13) decomposes the solution $w(x,t)$ into a summation of the spherical mean $\mathcal{U}(x,r;f)$ of function f.

On the other hand, we can also decompose the spherical mean $\mathcal{U}(x,r;f)$ into solutions of the standard wave equation; namely, we have the following inverse of the above relation (3.13).

THEOREM 3.3 (Courant and Hilbert [14], page 684). *Let $w(x,t) = \mathcal{W}(x,t;\{f,0\})$ be a solution of the wave equation* (3.12) *with the initial data $\{f,0\}$. Then we can decompose the spherical mean $\mathcal{U}(x,r;f)$ into the following summation of wave solutions:*

$$\mathcal{U}(x,r;f) = \frac{2\omega_{n-1}}{\omega_n}\frac{1}{r^{n-2}}\int_0^r \left(r^2-t^2\right)^{\frac{n-3}{2}}\mathcal{W}(x,t;\{f,0\})\,\mathrm{d}t \tag{3.14a}$$

$$= \frac{2\omega_{n-1}}{\omega_n}\int_0^1 \left(1-t^2\right)^{\frac{n-3}{2}}\mathcal{W}(x,rt;\{f,0\})\,\mathrm{d}t. \tag{3.14b}$$

Furthermore, when the initial data are $\{f,g\}$, we have

$$\mathcal{U}(x,r;f) = \frac{\omega_{n-1}}{\omega_n}\frac{1}{r^{n-2}}\int_{-r}^r \left(r^2-t^2\right)^{\frac{n-3}{2}}\mathcal{W}(x,t;\{f,g\})\,\mathrm{d}t. \tag{3.15}$$

Since the weight $(r^2-t^2)^{\frac{n-3}{2}}$ of the integrand in formula (3.14a) is rational in t for odd n and irrational for even n, this expression behaves differently accordingly. Although there is a singular factor r^{2-n} for all the above formulas as $r\to 0$, we can carry out a change of variables so that the variable r appears in the function $w(x,rt)$ only; see (3.14b). Hence, the spherical mean of a function can be obtained from solutions of the standard wave equation (3.12) and the relation (3.14).

A specific case. Now we consider the particular case, $n=2$, to illustrate how to evaluate the integral (3.14a). Consequently, the integrand in formula (3.14) is singular with order $-\frac{1}{2}$, which leads us to rewrite the formula as the following:

$$\mathcal{U}(x,r;f) = \frac{2\omega_1}{\omega_2}\frac{1}{r^2}\int_0^r \sqrt{r^2-t^2}\Big(2\,\mathcal{W}(x,t;\{f,0\}) + t\,\partial_t\mathcal{W}(x,t;\{f,0\})\Big)\,\mathrm{d}t. \tag{3.16}$$

Since the integral operator defined by the integral (3.16) is of the Volterra type, we propose to truncate the power-series expansion of the Volterra integral kernel to obtain an approximation of finite terms so that we can evaluate the resulting approximate integral efficiently.

Let $\epsilon > 0$ be an appropriate constant. Then for any t such that $0 \leqslant t \leqslant r - \epsilon < r$, we have

(3.17)
$$\sqrt{r^2 - t^2} = r\Big(1 - \frac{t^2}{r^2}\Big)^{\frac{1}{2}} = r\bigg[1 + \frac{\frac{1}{2}}{1!}\Big(-\frac{t^2}{r^2}\Big)^1 + \frac{\frac{1}{2}(-\frac{1}{2})}{2!}\Big(-\frac{t^2}{r^2}\Big)^2 + \cdots + \binom{s}{\frac{1}{2}}\Big(-\frac{t^2}{r^2}\Big)^s + \cdots\bigg],$$

where the binomial coefficient $\binom{s}{\frac{1}{2}} = \frac{\Gamma(\frac{3}{2})}{\Gamma(s+1)\Gamma(\frac{3}{2}-s)}$. Thus, we split the integral (3.16) into two parts,

$$\begin{aligned}\mathcal{U}(x, r; f) \;&=\; \frac{2\omega_1}{\omega_2}\bigg(\frac{1}{r^2}\int_0^{r-\epsilon} \sqrt{r^2 - t^2}\,\mathcal{V}(t)\,\mathrm{d}t + \frac{1}{r^2}\int_{r-\epsilon}^{r} \sqrt{r^2 - t^2}\,\mathcal{V}(t)\,\mathrm{d}t\bigg)\\ &:=\; \frac{2\omega_1}{\omega_2}\big(\,(\mathrm{I}) + (\mathrm{II})\,\big),\end{aligned}$$

where $\mathcal{V}(t) := 2\,\mathcal{W}(x, t; \{f, 0\}) + t\,\partial_t \mathcal{W}(x, t; \{f, 0\})$. Then, for part (I), we obtain

(3.18)
$$(\mathrm{I}) = \frac{1}{r}\int_0^{r-\epsilon} \mathcal{V}(t)\,\mathrm{d}t - \frac{1}{2}\frac{1}{r^3}\int_0^{r-\epsilon} t^2\,\mathcal{V}(t)\,\mathrm{d}t + \cdots + (-1)^s\binom{s}{\frac{1}{2}}\frac{1}{r^{2s+1}}\int_0^{r-\epsilon} t^{2s}\,\mathcal{V}(t)\,\mathrm{d}t + \cdots,$$

and we can evaluate each term $\int_0^{r-\epsilon} t^{2s}\,\mathcal{V}(t)\,\mathrm{d}t$ efficiently, in which the integrand $t^{2s}\,\mathcal{V}(t)$ does not depend on the variable r, which is in contrast to the integrand $\sqrt{r^2 - t^2}\,\mathcal{V}(t)$ of (3.16). For part (II), we choose ϵ small enough such that the numerical quadrature over a small interval $(r - \epsilon, r)$ is accurate. Moreover, we may choose ϵ to balance the errors from part (I) and part (II) so that the overall accuracy requirement is satisfied.

Therefore, we have an efficient approximation for evaluating the integral (3.16) when $n = 2$,

(3.19)
$$\mathcal{U}(x, r; f) \approx \frac{2\omega_1}{\omega_2}\bigg(\sum_{s=0}^{S}(-1)^s\binom{s}{\frac{1}{2}}\frac{1}{r^{2s+1}}\int_0^{r-\epsilon} t^{2s}\,\mathcal{V}(t)\,\mathrm{d}t + \frac{1}{r^2}\int_{r-\epsilon}^{r} \sqrt{r^2 - t^2}\,\mathcal{V}(t)\,\mathrm{d}t\bigg),$$

where the constants S and ϵ are to be determined in computation.

General cases. When $n = 1$, the spherical mean is simply the solution of the wave equation as shown in Darboux's equation (3.11). When $n \geqslant 2$ is *even*, we may apply the same strategy as for $n = 2$ (illustrated above) to compute the integral (3.14a). When $n \geqslant 3$ is *odd*, the integration weight $(r^2 - t^2)^{\frac{n-3}{2}}$ in the integral (3.14a) can be expanded as a polynomial of finite terms in the form of $r^k t^j$, where k and j are nonnegative integers so that the resulting integrals can be evaluated rapidly.

3.2.2. Solving Darboux's equation directly. Another way to generate the spherical mean $\mathcal{U}(x, r; f)$ of a function f is to solve Darboux's equation (3.11) directly. But since there is a singular term $\frac{n-1}{r}\partial_r u(x, r)$ in (3.11), we have to design our method to treat this singularity when r is close to the origin. Fortunately, since r is a time-like variable, the singularity only matters initially and can be removed as shown below.

We use a change of variables to remove this singularity. Let $r^2 = 4\rho$ so that we

have $\frac{1}{r}\partial_r = \frac{1}{2}\partial_\rho$. We also have that

$$\partial_r^2 u = r^2 \frac{1}{r}\partial_r\left(\frac{1}{r}\partial_r u\right) + \frac{1}{r}\partial_r u = \rho\partial_\rho^2 u + \frac{1}{2}\partial_\rho u, \quad \frac{n-1}{r}\partial_r u = \frac{n-1}{2}\partial_\rho u, \tag{3.20}$$

and

$$\rho\partial_\rho^2 u + \frac{n}{2}\partial_\rho u = \Delta_x u \tag{3.21}$$

according to Darboux's equation (3.11).

Furthermore, we assume that

$$u(x,r) = \sum_{k=0}^{\infty} u_k(x)\Big(\frac{r^2}{4}\Big)^k = \sum_{k=0}^{\infty} u_k(x)\rho^k \tag{3.22}$$

is a power series in the variable r for small enough r. Thus, it yields

$$\sum_{k=1}^{\infty} k\big(k-1+\frac{n}{2}\big)u_k(x)\rho^{k-1} = \sum_{k=1}^{\infty} \Delta_x u_{k-1}(x)\rho^{k-1}, \tag{3.23}$$

and the corresponding initial datum is

$$u_0(x) = f(x). \tag{3.24}$$

Comparing coefficients on the two sides of the above formula, we now get

$$k\big(k-1+\frac{n}{2}\big)u_k(x) = \Delta_x u_{k-1}(x), \tag{3.25}$$

leading to

$$\begin{aligned} u_k(x) &= \frac{\Delta_x u_{k-1}(x)}{k\left(k-1+\frac{n}{2}\right)} = \frac{(\Delta_x)^k f(x)}{k!\,\frac{n}{2}\left(1+\frac{n}{2}\right)\cdots\left(k-1+\frac{n}{2}\right)} \\ &= \frac{\Gamma\left(\frac{n}{2}\right)}{\Gamma(k+1)\,\Gamma\left(k+\frac{n}{2}\right)}(\Delta_x)^k f(x). \end{aligned} \tag{3.26}$$

Therefore, we obtain the power series

$$u(x,r) = \sum_{k=0}^{\infty} \frac{\Gamma\left(\frac{n}{2}\right)}{\Gamma(k+1)\,\Gamma\left(k+\frac{n}{2}\right)}(\Delta_x)^k f(x)\Big(\frac{r^2}{4}\Big)^k \tag{3.27}$$

in r as a solution of Darboux's equation for small enough r. Afterward, we may switch to solve Darboux's equation directly.

We mention in passing that we can generate the spherical mean $\mathcal{U}(x,r;f)$ according to its original definition (3.1). It indicates that, for any $x \in \mathbb{R}^n$ and $r \geqslant 0$, we need to compute the average over a sphere of radius r at the center x; however, in practice this is not an easy task on a uniform grid. The most efficient way for generating spherical means is to utilize the relation (3.14) with solutions of the standard wave equation or to solve Darboux's equation (3.11) directly with an effective strategy for small r.

3.2.3. Asymptotic behavior of spherical means as $r \to \infty$. Now we characterize the asymptotic behavior of the solution of Darboux's equation, i.e., $\mathcal{U}(x, r; f)$ as $r \to \infty$.

We first consider the case $n = 1$. If we assume that the initial datum $f(x)$ of (3.11) has the asymptotic expansion

$$f(x) \sim \sum_{k=0}^{\infty} \frac{a_k}{x^k}, \quad x \to \infty, \tag{3.28}$$

then, as shown on page 824 of [41], we have that

$$\mathcal{U}(x, r; f) \sim \sum_{k=0}^{\infty} \frac{c_k(x)}{r^{2k}}, \quad r \to \infty, \tag{3.29}$$

where $c_0(x) = a_0$ and $c_k(x) = \sum_{\ell=0}^{2k-1} \binom{2k-1}{\ell} a_{2k-\ell}(-x)^\ell$ is a polynomial of degree $2k-1$ in the variable x.

Therefore, if there is a $k^* \neq 0$ such that $a_{k^*} \neq 0$, and $a_k = 0$ for any $k \neq k^*$, implying that f has the following algebraic decaying,

$$f(x) \sim \frac{a_{k^*}}{x^{k^*}}, \quad x \to \infty, \tag{3.30}$$

then we have that

$$\mathcal{U}(x, r; f) \sim \frac{a_{k^*}}{r^{k^*}} \sum_{k=0}^{\infty} \frac{\binom{k^*+k-1}{k}(-x)^k}{r^k} = \mathcal{O}(r^{-k^*}), \quad r \to \infty. \tag{3.31}$$

This estimate says that the spherical mean depends on the order k^* of the variable x in the function $f(x)$.

Next we consider the case $n \geqslant 2$. Denoting $\mu := \frac{n-2}{2} \geqslant 0$, we have the following expansion of the spherical mean (page 77 of [25]):

$$\mathcal{U}(x, r; f) = P_\mu\big(r\sqrt{-\Delta_x}\,\big) f(x), \tag{3.32}$$

where $P_\mu(s) = \Gamma(\mu+1)\left(\frac{2}{s}\right)^\mu J_\mu(s)$ is a normalized Bessel function with $P_\mu(0) = 1$ and $J_\mu(s)$ is the Bessel function of the first kind. Indeed, this expansion should be understood in the sense of expanding it into a powers series of $r\sqrt{-\Delta_x}$ and having each term act separately on $f(x)$. Then, according to the classical asymptotic expansion of the Bessel function $J_\mu(s) \sim \sqrt{2/(\pi s)}\cos(s - (2\mu+1)\pi/4)$ as $s \to \infty$, we could obtain the following crude asymptotic expansion in the variable r:

$$\mathcal{U}(x, r; f) \sim c_\mu(x)\, r^{-\mu-\frac{1}{2}}, \quad r \to \infty, \tag{3.33}$$

where $c_\mu(x)$ is a function of x. Therefore, if we only consider the spherical mean $\mathcal{U}(x, r; f)$ as a function of r, then we can assume that the spherical mean has the asymptotic behavior

$$\mathcal{U}(x, r; f) \sim \mathcal{O}(r^{-\beta}), \quad r \to \infty \tag{3.34}$$

with an order $\beta > 0$, where a rough estimate of β is $\frac{n-1}{2}$ when $n \geqslant 2$.

4. Numerical algorithms.

4.1. A sketch of numerical algorithms. As shown by Theorem 3.1, if the spherical mean of a function is given, then we could reduce any n-dimensional fractional Laplacian (2.1) to the 1-D one. Therefore, at first we should generate the spherical mean according to the relation between the solution of Darboux's equation and that of the standard wave equation, or we should solve Darboux's equation with a given initial datum directly to obtain the spherical mean of a function. Then a 1-D fractional Laplacian acts on the spherical mean of the underlying function to produce the multi-D fractional Laplacian of the given function.

Furthermore, Theorem 3.2, Corollaries 3.1 and 3.2, also show that any n-dimensional fractional derivative or integral of a function can be obtained from the corresponding 1-D fractional operator if the spherical mean of the underlying function is given. Consequently, we may have the following algorithm to implement the action of a multi-D fractional operator to a given function.

Algorithm 1. A numerical method for fractional operators in multi-D spaces.

Input: a function f, the space dimension n, and a parameter α.
Output: a function $A_x^\alpha f$ for $x \in \mathbb{R}^n$.

0. Given the space dimension n, a function f, and a parameter α, compute the multi-D fractional operator A_x^α for $x \in \mathbb{R}^n$.

1A. Solve the standard wave equation (3.12) with the initial data $\{f, 0\}$, and give a solution $w(x,t) = \mathcal{W}(x,t;\{f,0\})$ for $x \in \mathbb{R}^n$ and $t \geqslant 0$. Then utilize the relation (3.14) to generate the spherical mean $\mathcal{U}(x,r;f)$ from the solution $\mathcal{W}(x,t;\{f,0\})$ for $x \in \mathbb{R}^n$ and $r \geqslant 0$.

1B. Or solve Darboux's equation (3.11) directly with the initial data $\{f,0\}$ and the power series (3.27) for small r, yielding a solution $u(x,r) = \mathcal{U}(x,r;f)$ as the spherical mean for $x \in \mathbb{R}^n$ and $r \geqslant 0$.

2. For each point $x \in \mathbb{R}^n$, the corresponding 1-D fractional operator A_r^α acts on the even function $\mathcal{U}(x,r;f)$ of r so that we have

$$A_x^\alpha f(x) = \Big[A_r^\alpha \mathcal{U}(x,r;f) \Big]\Big|_{r=0}. \tag{4.1}$$

In the above algorithmic sketch, the operator A_r^α is chosen according to the operator A_x^α:

i. The fractional Laplacian:
Set $A_r^\alpha = \left(-\partial_r^2\right)^{\frac{\alpha}{2}}$ for $A_x^\alpha = \left(-\Delta_x\right)^{\frac{\alpha}{2}}$ with $\alpha \in (0,2)$; see the formula (3.3) or (3.6).

ii. The extended fractional Laplacian:
Set $A_r^\alpha = \left(-\partial_r^2\right)_j^{\frac{\alpha}{2}}$ for $A_x^\alpha = \left(-\Delta_x\right)_j^{\frac{\alpha}{2}}$ with $\alpha \in (0,j)$ and $j = 2,4,6,\ldots$; see the formula (3.5a) or (3.7a).

iii. The Riesz potential operator:
Set $A_r^\alpha = R_r^\alpha$ for $A_x^\alpha = R_x^\alpha = \left(-\Delta_x\right)^{-\frac{\alpha}{2}}$ with $\alpha \in (0,n)$; see the formula (3.5b) or (3.7b).

In the following subsections, we will detail numerical schemes for each step of the above method.

4.2. Generating the spherical mean of a given function. To generate spherical means, we first need to solve the standard wave equation (3.12) or Darboux's equation (3.11) with the initial data $\{f, 0\}$, yielding the solution $w(x,t) = \mathcal{W}(x,t;\{f,0\})$ or the solution $u(x,r) = \mathcal{U}(x,r;f)$. There are many efficient numerical methods to solve the wave equation or Darboux's equation in the entire space $\mathbb{R}^n$ with $t, r \geqslant 0$.

For the sake of simplicity, we assume that the initial data are compactly supported. We solve the wave equation or Darboux's equation (wave-like equation) with second-order finite difference in both space and time, where we adopt the perfectly matched layer (PML) absorbing boundary condition to truncate the unbounded computational domain $\mathbb{R}^n$ into a bounded domain. Since a space-time staggered grid is utilized inside the absorbing layer, both the solution $w(x,t)$ and its derivative $\partial_t w(x,t)$ are available to us right away, which are needed in the formula (3.16) when $n = 2$. The Courant–Friedrichs–Lewy (CFL) condition will be used for choosing the step-length in time.

We first consider step (1A) of the method. Given a uniform grid with the grid spacing h and the time step $\tau \leqslant C_{\mathrm{CFL}} h$, where a staggered grid is used here and C_{CFL} is the CFL constant, we denote w_i^k as a numerical approximation of $w(x_i, t_k)$ at position $x_i \in \mathbb{R}^n$ and time $t_k = k\tau$ for $k \geqslant 0$ and $\widehat{w}_i^{k+\frac{1}{2}}$ as an approximation of $\partial_t w(x_i, t_{k+\frac{1}{2}})$. Thus, we obtain that

$$\begin{aligned} w_i^k - w(x_i, t_k) &\approx \mathcal{O}\left(\tau^2\right) + \mathcal{O}\left(h^2\right), \\ \widehat{w}_i^{k+\frac{1}{2}} - \partial_t w(x_i, t_{k+\frac{1}{2}}) &\approx \mathcal{O}\left(\tau^2\right) + \mathcal{O}\left(h^2\right). \end{aligned} \tag{4.2}$$

Next, we generate the spherical mean $\mathcal{U}(x,r;f)$ according to the formula (3.14). We apply the composite trapezoidal rule to carry out numerical integration. The grid for the variable r is the same as that for the variable t, i.e., $r_k = t_k = k\tau$. Denoting u_i^k as the computed spherical mean at position x_i of radius r_k, we have the following numerical formula: For $k = 0$,

$$u_i^0 = w_i^0 = f_i = f(x_i); \tag{4.3}$$

for $k \geqslant 1$,

(4.4)

$$u_i^k = \begin{cases} w_i^k, & n = 1, \\ \dfrac{2\omega_1}{\omega_2} \displaystyle\sum_{s=0}^{S} (-1)^s \binom{s}{\frac{1}{2}} \frac{1}{k^{2s+1}} \left(\sum_{\ell=0}^{k-\theta} a_\ell \, \ell^{2s} \, 2\, w_i^\ell + \sum_{\ell=0}^{k-\theta-1} b_\ell \, (\ell + \tfrac{1}{2})^{2s+1} \, \tau \, \widehat{w}_i^{\ell+\frac{1}{2}} \right) \\ \quad + \dfrac{2\omega_1}{\omega_2} \dfrac{1}{k^2} \left(\displaystyle\sum_{\ell=k-\theta}^{k} a_\ell \sqrt{k^2 - \ell^2}\, 2\, w_i^\ell + \sum_{\ell=k-\theta}^{k-1} b_\ell \sqrt{k^2 - (\ell + \tfrac{1}{2})^2}\, (\ell + \tfrac{1}{2}) \tau \, \widehat{w}_i^{\ell+\frac{1}{2}} \right), & n = 2, \\ \dfrac{2\omega_{n-1}}{\omega_n} \dfrac{1}{k^{n-2}} \displaystyle\sum_{\ell=0}^{k} a_\ell \left(k^2 - \ell^2\right)^{\frac{n-3}{2}} w_i^\ell, & n \geqslant 3, \end{cases}$$

where the coefficients $a_0 = a_k = \frac{1}{2}$, $a_\ell = 1$ for any $\ell \neq 0$ or k, and $b_0 = b_{k-1} = \frac{3}{4}$, $b_\ell = 1$ for any $\ell \neq 0$ or $k-1$. Herein, when $n = 2$, the small value ϵ in (3.19) is chosen as $\epsilon = \theta\tau$, where θ is a constant to be chosen in computation. As mentioned before,

since the integral is singular when $n = 2$, we rewrite the original formula (3.14) into the formula (3.16) by using the function $\partial_t w(x,t)$. Using the estimate (4.2) and the fact that the accuracy of the composite trapezoidal rule is second-order, we have that

$$u_i^k - \mathcal{U}(x_i, r_k; f) \approx \mathcal{O}\left(\tau^2\right) + \mathcal{O}\left(h^2\right). \tag{4.5}$$

We next consider step (1B) of the method. Since the variable r is time-like in Darboux's equation, we can also use the second-order finite difference scheme to obtain the solution u_i^k numerically. In particular, for r small enough, we utilize the power series (3.27) to obtain a reliable approximation. This series will be truncated so that only the first three terms are used. Thus, we can also obtain a second-order accurate approximation u_i^k to the spherical mean as above (4.5).

In general, we can use high-order numerical schemes to solve wave equations and carry out numerical integrations so that the accuracy order of u_i^k could be improved to be $\mathcal{O}(\tau^p) + \mathcal{O}(h^q)$, where $p, q \geqslant 2$, but we choose to explore this in a future project for the sake of clarity.

REMARK 4.1. We remark that, in general, it is not an easy task to generate the spherical mean $\mathcal{U}(x, r; f)$ on a uniform grid from a given function f since we need to compute the average over a sphere according to its original definition (3.1). When the function f is periodic or compactly supported in an n-dimensional torus $\mathbb{T}^n$, the work in [20] considered a spectral discretization via trigonometric polynomials, where most of the computation can be done via nonequispaced fast Fourier transforms [26] or butterfly sparse fast Fourier transforms [28, 48] when $n = 3$. However, if the function is not periodic or has an algebraically decaying tail, then it seems that the most efficient way to compute spherical means on a uniform grid is to solve Darboux's wave equation directly or to solve a wave equation and use the decomposition principle to recover the spherical mean via the relation (3.14).

REMARK 4.2. Although both of our proposed approaches work equally well for constructing spherical means, they have different features. In terms of decomposition of spherical means into wave solutions (3.14), we need to carry out numerical integrations of wave solutions. Since we have not optimized this numerical quadrature process yet at the current stage, the computational cost is slightly high to obtain high-order accuracy. Taking the Gaussian quadrature rule as an example, we need to compute the wave solutions on a set of Gaussian nodes t_k^*. In terms of solving Darboux's equation directly, we first treat the singular term in Darboux's equation carefully via a power series (3.27) when r is small enough, then we obtain a reliable approximation by solving the wave-like equation so that the overall computational cost is low. However, the propagation of the initial error in the power-series truncation through this wave-like equation will have an effect on the accuracy order of the schemes.

4.3. Approximating the 1-D extended fractional operator. Although several numerical schemes are available for computing the 1-D fractional derivative or integral, we will adopt the schemes in [16, 23] which are suitable to our setting in terms of spherical means.

We start with the fractional derivatives. Recall that the fractional Laplacian (2.1) or, more generally, the extended fractional Laplacian (2.9) in the 1-D space is defined by

$$\left(-\partial_r^2\right)_j^{\frac{\alpha}{2}} u(r) = C_{1,\alpha,j} \text{ p.v.} \int_{\mathbb{R}^1} \frac{\mathcal{D}_j(r, \rho; u)}{|\rho|^{1+\alpha}} \, \mathrm{d}\rho, \quad r \in \mathbb{R}^1, \tag{4.6}$$

where $(C_{1,\alpha,j})^{-1} = (-1)^{\frac{j}{2}} 2^{j-\alpha+1} \int_0^\infty (\sin t)^j t^{-1-\alpha}\,\mathrm{d}t$ with $\alpha \in (0, j)$ and $j = 2, 4, 6, \ldots$. If $j = 2$, we recover the fractional Laplacian (2.1) when the space dimension is one.

Following [16, 23], we take $\tau < 1$ and split the above Cauchy principal-valued integral into two parts,

$$\begin{aligned}\left(-\partial_r^2\right)_j^{\frac{\alpha}{2}} u(r) &= C_{1,\alpha,j}\left(\text{p.v.}\int_{|\rho|\leqslant\tau} \frac{\mathcal{D}_j(r,\rho;u)}{|\rho|^{1+\alpha}}\,\mathrm{d}\rho + \int_{|\rho|>\tau} \frac{\mathcal{D}_j(r,\rho;u)}{|\rho|^{1+\alpha}}\,\mathrm{d}\rho\right),\\ &:= C_{1,\alpha,j}\left(\, I_{\mathrm{s}}[u](r) + I_{\mathrm{r}}[u](r)\,\right), \qquad r \in \mathbb{R}^1,\end{aligned} \tag{4.7}$$

where $I_{\mathrm{s}}[u](r)$ and $I_{\mathrm{r}}[u](r)$ denote the singular and regular part, respectively. We will treat the two parts separately.

For any integer $m \geqslant 0$ and $\nu \in (0, 1]$, we denote the *Hölder space* of continuous functions on $\mathbb{R}^1$ by

$$C^{m,\nu}(\mathbb{R}^1) := \Big\{\, u(r) \in C^m(\mathbb{R}^1) \;:\; \max_{\substack{0\leqslant k\leqslant m\\ k\in\mathbb{N}}} \sup_{\substack{r,\rho\in\mathbb{R}^1\\ r\neq\rho}} \frac{\left|u^{(k)}(r) - u^{(k)}(\rho)\right|}{|r-\rho|^{\nu}} < \infty \Big\}, \tag{4.8}$$

where $C^m(\mathbb{R}^1)$ is the space consisting of all functions u which, together with all their derivatives $u^{(k)}$ of orders $k \leqslant m$, are continuous on $\mathbb{R}^1$, and this space is equipped with the norm given by

$$\|u\|_m := \max_{0\leqslant k\leqslant m} \sup_{r\in\mathbb{R}^1} \left|u^{(k)}(r)\right|. \tag{4.9}$$

Furthermore, in order to estimate the accuracy order of the scheme, we have to assume that the function u is sufficiently smooth such as $u(r) \in C^{m,\nu}(\mathbb{R}^1)$ in general. In fact, [16] considered the Hölder space with $m = 1, 3$ and $\nu = \frac{\alpha}{2}$, and [23] proved results for $C^m(\mathbb{R}^1)$ with $m = 4$.

4.3.1. The singular part $I_{\mathrm{s}}[u](r)$. We treat the singular part $I_{\mathrm{s}}[u](r)$ on the interval $[-\tau, \tau]$ first. We extend the original schemes in [16, 23] for $j = 2$ to any even $j > \alpha > 0$. Given an even number $j > \alpha > 0$ and any $\gamma \in (\alpha, 2]$, if $u(r) \in C^{m,\nu}(\mathbb{R}^1)$, then the function $\phi_{\gamma,j}(r,\rho) := \rho^{-\gamma}\mathcal{D}_j(r,\rho;u)$ satisfies that, for any integer $0 \leqslant k \leqslant m$, there exists a constant $C > 0$ such that the estimate

$$\left|\partial_\rho^k\, \phi_{\gamma,j}(\cdot,\rho)\right| \leqslant C\rho^{m+\nu-\gamma-k} \tag{4.10}$$

holds. This property can be proved by directly applying Taylor's theorem; see a similar result in Lemma 3.3 of [16]. Thus, using (4.10) with $k = 0$, we have

$$\begin{aligned} I_{\mathrm{s}}[u](r) &= \ \text{p.v.}\int_{-\tau}^{\tau} \mathcal{D}_j(r,\rho;u)\,|\rho|^{-1-\alpha}\,\mathrm{d}\rho\\ &= 2\int_0^\tau \mathcal{D}_j(r,\rho;u)\rho^{-1-\alpha}\,\mathrm{d}\rho\\ &= 2\int_0^\tau \rho^{-\gamma}\mathcal{D}_j(r,\rho;u)\rho^{\gamma-1-\alpha}\,\mathrm{d}\rho\\ &= \kappa_\gamma\tau^{-\gamma}\mathcal{D}_j(r,\tau;u)\int_0^\tau \rho^{\gamma-1-\alpha}\,\mathrm{d}\rho\\ &\quad + \int_0^\tau \left(2\rho^{-\gamma}\mathcal{D}_j(r,\rho;u) - \kappa_\gamma\tau^{-\gamma}\mathcal{D}_j(r,\tau;u)\right)\rho^{\gamma-1-\alpha}\,\mathrm{d}\rho\\ &= \kappa_\gamma\frac{\tau^{-\alpha}}{\gamma-\alpha}\,\mathcal{D}_j(r,\tau;u) + \mathcal{O}\left(\tau^{m+\nu-\alpha}\right), \end{aligned} \tag{4.11}$$

where the constant $\kappa_\gamma = 1$ for $\gamma \in (\alpha, 2)$ while $\kappa_\gamma = 2$ if $\gamma = 2$. Notice that the jth-order central difference $\mathcal{D}_j(r,\rho;u)$ is an even function of ρ when the order j is even. Thus, in fact, in the last line of the above equation, we just use the function $\kappa_\gamma \tau^{-\gamma}\mathcal{D}_j(r,\tau;u)$ to approximate the integrand $2\rho^{-\gamma}\mathcal{D}_j(r,\rho;u)$ within the interval $[-\tau,\tau]$ and obtain a singular term $|\rho|^{\gamma-1-\alpha}$ of order lower than one since $\gamma - 1 - \alpha > -1$. If $u(r) \in C^m(\mathbb{R}^1)$, then we can only obtain the accuracy order $\mathcal{O}(\tau^{m-\alpha})$ in the interval $[-\tau,\tau]$.

4.3.2. The regular part for $I_{\mathrm{r}}[u](r)$. Two numerical approaches are available to approximate the regular part of the integral (4.6): the composite weighted trapezoidal rule [16] and the interpolation-based quadrature [23]. To simplify notations, we denote $\widetilde{u}(\rho) := \mathcal{D}_j(r,\rho;u)$, which is an even function of ρ. We also introduce a uniform grid $\rho_\ell = \ell\tau$ and $\ell \geqslant 0$ as used in solving wave equations.

Consequently, letting $\widetilde{u}(\rho) \in C^{m,\nu}(\mathbb{R}^1)$ and using the composite weighted trapezoidal rule [16], we have

$$
\begin{aligned}
I_{\mathrm{r}}[u](r) &= \int_{|\rho|>\tau} \widetilde{u}(\rho)\,|\rho|^{-1-\alpha}\,\mathrm{d}\rho \\
&= 2\int_{\rho>\tau} \widetilde{u}(\rho)\rho^{-1-\alpha}\,\mathrm{d}\rho \\
&= \sum_{\ell=1}^{\infty}\int_{\rho_\ell}^{\rho_{\ell+1}} \left(\rho_\ell^{-\gamma}\widetilde{u}(\rho_\ell) + \rho_{\ell+1}^{-\gamma}\widetilde{u}(\rho_{\ell+1})\right)\rho^{\gamma-1-\alpha}\,\mathrm{d}\rho \\
&\quad + \sum_{\ell=1}^{\infty}\int_{\rho_\ell}^{\rho_{\ell+1}} \left(2\rho^{-\gamma}\widetilde{u}(\rho) - \rho_\ell^{-\gamma}\widetilde{u}(\rho_\ell) - \rho_{\ell+1}^{-\gamma}\widetilde{u}(\rho_{\ell+1})\right)\rho^{\gamma-1-\alpha}\,\mathrm{d}\rho \\
&= \sum_{\ell=1}^{\infty} W_{\ell,\gamma}^{\alpha,\tau}\,\widetilde{u}(\rho_\ell) + \mathcal{O}\left(\tau^{m+\nu-\alpha}\right),
\end{aligned}
\tag{4.12}
$$

where $W_{\ell,\gamma}^{\alpha,\tau} := \frac{\tau^{-\alpha}}{\gamma-\alpha}\ell^{-\gamma}\left((\ell+1)^{\gamma-\alpha} - (\ell-1)^{\gamma-\alpha}\right)$. Moreover, following [16], we can obtain the accuracy order of the weighted trapezoidal rule with the weight function $\rho^{\gamma-1-\alpha}$ in the last line of the above formula; to do that, we will use an extension of the weighted Montgomery identity [27] and the estimate (4.10) of $\phi_{\gamma,j}(r,\rho) = \rho^{-\gamma}\widetilde{u}(\rho)$ with $k \geqslant 1$, where the parameter γ is chosen to be $\gamma = 2$ or $1 + \frac{\alpha}{2}$ as in [16].

Similarly, if $\widetilde{u}(\rho) \in C^m(\mathbb{R}^1)$, then we obtain by using the interpolation-based quadrature rule [23]

(4.13)

$$
\begin{aligned}
I_{\mathrm{r}}[u](r) &= \int_{|\rho|>\tau} \widetilde{u}(\rho)\,|\rho|^{-1-\alpha}\,\mathrm{d}\rho \\
&= 2\int_{\rho>\tau}\left(\sum_{\ell=0}^{\infty}\widetilde{u}(\rho_\ell)q_\ell(\rho)\right)\rho^{-1-\alpha}\,\mathrm{d}\rho + 2\int_{\rho>\tau}\left(\widetilde{u}(\rho) - \sum_{\ell=0}^{\infty}\widetilde{u}(\rho_\ell)q_\ell(\rho)\right)\rho^{-1-\alpha}\,\mathrm{d}\rho \\
&= \sum_{\ell=0}^{\infty} Q_{\ell,m}^{\alpha,\tau}\,\widetilde{u}(\rho_\ell) + \mathcal{O}\left(\tau^{m-\alpha}\right),
\end{aligned}
$$

where we assume that the integral $Q_{\ell,m}^{\alpha,\tau} := 2\int_{\rho>\tau} q_\ell(\rho)\rho^{-1-\alpha}\,\mathrm{d}\rho$ exists, the accuracy order of the interpolation is $\mathcal{O}(\tau^m)$, and the basis function q_ℓ satisfies $q_\ell(\rho_k) = \delta_{k\ell}$ with $\delta_{k\ell}$ being the Kronecker delta function. The simplest basis function for linear interpolation can be taken to be a shifted and scaled hat function on the interval $[-\tau,\tau]$, where the order of accuracy is $m = 2$.

In general, since $\widetilde{u}(\rho) = \mathcal{D}_j(r, \rho; u)$, we just need to make the same assumption as $u(r) \in C^{m,\nu}(\mathbb{R}^1)$ or $C^m(\mathbb{R}^1)$ to apply the composite weighted trapezoidal rule or the interpolation-based quadrature rule, respectively.

4.3.3. Treating the truncated tail. Since the discretized regular part involves a summation of an infinite number of terms, we will truncate this infinite summation into a finite sum of the first L terms.

Therefore, using the composite weighted trapezoidal rule and taking the first $L+1$ data points, we obtain a truncated term for the regular part of the integral (4.6), that is,

$$\int_{\rho>\rho_L} \widetilde{u}(\rho)\rho^{-1-\alpha}\,\mathrm{d}\rho \approx \sum_{\ell=L+1}^{\infty} \int_{\rho_\ell}^{\rho_{\ell+1}} \left(\rho_\ell^{-\gamma}\widetilde{u}(\rho_\ell) + \rho_{\ell+1}^{-\gamma}\widetilde{u}(\rho_{\ell+1})\right)\rho^{\gamma-1-\alpha}\,\mathrm{d}\rho. \tag{4.14}$$

Or, similarly, using the interpolation-based quadrature, we have an approximation of $\widetilde{u}$ in the form that $\widetilde{u}(\rho) \approx \sum_{\ell=0}^{L} \widetilde{u}(\rho_\ell) q_\ell(\rho)$ on the interval $[0, \rho_L]$, yielding

$$\int_{\rho>\rho_L} \widetilde{u}(\rho)\rho^{-1-\alpha}\,\mathrm{d}\rho \approx \int_{\rho>\tau} \left(\sum_{\ell=L+1}^{\infty} \widetilde{u}(\rho_\ell) q_\ell(\rho)\right)\rho^{-1-\alpha}\,\mathrm{d}\rho. \tag{4.15}$$

However, according to the estimate in (2.8) and the tail estimate in (3.34), generically the function $\widetilde{u}$ has an algebraically decaying tail so that the contribution of the above truncated terms cannot be ignored.

If we assume that $\widetilde{u}(\rho) \sim \rho^{-\beta}$ as $\rho \to \infty$ with an order $\beta > 0$, where the order β can be estimated from the function $\widetilde{u}$ itself, then there is a constant ρ^* satisfying $\rho_L \leqslant \rho_{L^*} \leqslant \rho^* < \rho_{L^*+1} < \infty$ so that the following holds:

$$\int_{\rho>\rho_L} \widetilde{u}(\rho)\rho^{-1-\alpha}\,\mathrm{d}\rho = \widetilde{u}(\rho_L)\int_{\rho_L}^{\rho^*} \rho^{-1-\alpha}\,\mathrm{d}\rho = \frac{\rho_L^{-\alpha}}{\alpha}\,\widetilde{u}(\rho_L) + \mathcal{O}\left(\rho_L^{-\alpha-\beta}\right). \tag{4.16}$$

In our case here, since $\widetilde{u}(\rho) = \mathcal{D}_j(r, \rho; u) = \mathcal{D}_j(r, \rho; \mathcal{U}(x, \cdot; f))$, we can estimate the order β from the order of the spherical mean $\mathcal{U}(x, r; f)$ in r. Roughly speaking, the order β equals the order of r of the spherical mean so that $\beta \approx \frac{n-1}{2}$ from the estimate (3.34).

Finally, assuming that $u(r) \in C^{m,\nu}(\mathbb{R}^1)$, we evaluate the integral (4.6) at the grid point $r_k = k\tau$, yielding

$$\begin{aligned} \left(-\partial_r^2\right)_j^{\frac{\alpha}{2}} u(r_k) &= C_{1,\alpha,j}\ \text{p.v.} \int_{\mathbb{R}^1} \frac{\mathcal{D}_j(r_k, \rho; u)}{|\rho|^{1+\alpha}}\,\mathrm{d}\rho \\ &= C_{1,\alpha,j} \sum_{\ell=1}^{L} \left(\widetilde{P}_{\gamma,\ell}^{\alpha,\tau} + P_\ell^{\alpha,\tau}\right)\mathcal{D}_j(r_k, \rho_\ell; u) + \mathcal{O}\left(\tau^{m+\nu-\alpha}\right), \end{aligned} \tag{4.17}$$

where the jth-order central difference is

$$\mathcal{D}_j(r_k, \rho_\ell; u) = \sum_{s=0}^{j} (-1)^s \binom{j}{s} u(r_k + (\tfrac{j}{2} - s)\rho_\ell) = \sum_{s=0}^{j} (-1)^s \binom{j}{s} u(r_{\left\{k+(\frac{j}{2}-s)\ell\right\}}). \tag{4.18}$$

Therefore, according to the estimate of the singular part on $\rho \in [-\tau, \tau]$ and the truncated term of the integral (4.6) for $|\rho| > \rho_L$, we have the following new weighting

constant $\widetilde{P}_{\gamma,\ell}^{\alpha,\tau} := \tau^{-\alpha}\left(\kappa_\gamma \frac{1}{\gamma-\alpha}\,\delta_{1\ell} + 2\frac{L^{-\alpha}}{\alpha}\,\delta_{L\ell}\right)$ to correct the original weight:

$$P_\ell^{\alpha,\tau} := \begin{cases} W_{\ell,\gamma}^{\alpha,\tau} = \dfrac{\tau^{-\alpha}}{\gamma-\alpha}\ell^{-\gamma}\left((\ell+1)^{\gamma-\alpha} - (\ell-1)^{\gamma-\alpha}\right) \\ \qquad \text{for the composite weighted trapezoidal rule,} \\ Q_{\ell,m}^{\alpha,\tau} = 2\displaystyle\int_{\rho>\tau} q_\ell(\rho)\rho^{-1-\alpha}\,\mathrm{d}\rho \\ \qquad \text{for the interpolation-based quadrature rule.} \end{cases} \tag{4.19}$$

In fact, balancing order estimates (4.16) and (4.17) suggests that we choose the truncated value ρ_L or the constant L according to

$$L \sim \mathcal{O}\left(\tau^{-\frac{m+\nu+\beta}{\alpha+\beta}}\right). \tag{4.20}$$

Remark 4.3. The weighting constant $Q_{\ell,m}^{\alpha,\tau}$ depends on the basis function q_ℓ used for interpolation. Moreover, the accuracy order of (4.17) is $\mathcal{O}(\tau^{m-\alpha})$ if $u(r) \in C^m(\mathbb{R}^1)$. In [23], the piecewise linear interpolation with $m = 2$ yields

$$Q_{\ell,2}^{\alpha,\tau} = \tau^{-\alpha}\begin{cases} F_2(\ell+1) - F_2(\ell) - F_1(\ell), & \ell = 1, \\ F_2(\ell+1) - 2F_2(\ell) + F_2(\ell-1), & \ell = 2,3,\ldots, \end{cases} \tag{4.21}$$

and the piecewise quadratic interpolation with $m = 3$ yields

$$Q_{\ell,3}^{\alpha,\tau} = \tau^{-\alpha}\begin{cases} F_3(\ell+2) - F_3(\ell) - \dfrac{1}{2}F_2(\ell+2) - \dfrac{3}{2}F_2(\ell) - F_1(\ell), & \ell = 1, \\ -2F_3(\ell+1) + 2F_3(\ell-1) + 2F_2(\ell+1) + 2F_2(\ell-1), & \ell = 2,4,\ldots, \\ F_3(\ell+2) - F_3(\ell-2) - \dfrac{1}{2}F_2(\ell+2) - 3F_2(\ell) - \dfrac{1}{2}F_2(\ell-2), & \ell = 3,5,\ldots. \end{cases} \tag{4.22}$$

Here, the functions $F_1(\ell)$, $F_2(\ell)$, and $F_3(\ell)$ are given by

$$F_1(\ell) = \frac{\ell^{-\alpha}}{-\alpha}, \quad F_2(\ell) = \begin{cases} \dfrac{\ell^{1-\alpha}}{-(1-\alpha)\alpha}, & \alpha \neq 1, \\ -\ln\ell, & \alpha = 1, \end{cases} \quad F_3(\ell) = \begin{cases} \dfrac{\ell^{2-\alpha}}{-(2-\alpha)(1-\alpha)\alpha}, & \alpha \neq 1, \\ \ell\,(1-\ln\ell\,), & \alpha = 1, \end{cases} \tag{4.23}$$

where $F_1 = F_2' = F_3''$.

Remark 4.4. As a comparison, the standard 1-D Laplacian operator $\left(-\partial_r^2\right)$ can be discretized by using the central-difference scheme. For a given grid point $r_k = k\tau$, denoting $u^k \approx u(r_k)$, we can approximate this negative Laplacian operator by

$$\begin{aligned} \left(-\partial_r^2\right)u(r_k) &= -\tau^{-2}\left(u^{k-1} - 2u^k + u^{k+1}\right) + \mathcal{O}\left(\tau^2\right) \\ &\approx \sum_{\ell=\pm1} \tau^{-2}\left(u^k - u^{k+\ell}\right). \end{aligned} \tag{4.24}$$

4.4. Multi-D fractional operator. According to Theorems 3.1 and 3.2, to apply the multi-D fractional Laplacian to a function f, we only need to evaluate the integral (4.6) at the origin $r_0 = 0$ as long as the spherical mean $u(r) = \mathcal{U}(x, r; f)$ is available.

We assume that the computed spherical mean u_i^k at position x_i of radius r_k has been computed by the formula (4.4) or by solving Darboux's equation directly. Let $\mathbf{T}_j^\alpha$ and $\mathbf{v}_i$ be two vectors of L components. Applying the formula (4.17) and Theorem 3.2, we obtain an estimate of the dot product of these two vectors,

$$\begin{aligned}\mathbf{T}_j^\alpha \cdot \mathbf{v}_i - (-\Delta_x)_j^{\frac{\alpha}{2}} f(x_i) &= \mathbf{T}_j^\alpha \cdot \mathbf{v}_i - d_{n,\alpha,j} \left[\left(-\partial_r^2\right)_j^{\frac{\alpha}{2}} \mathcal{U}(x_i, r; f) \right] \Big|_{r=r_0} \\ &\approx \mathcal{O}\left(\tau^{m+\nu-\alpha}\right) + \mathcal{O}\left(\tau^2\right) + \mathcal{O}\left(h^2\right),\end{aligned} \tag{4.25}$$

where the given order j is even, the ℓth component of the vector $\mathbf{T}_j^\alpha$ is

$$\left[\mathbf{T}_j^\alpha\right]_\ell = \frac{\omega_n}{2} C_{n,\alpha,j} \left(\widetilde{P}_{\gamma,\ell}^{\alpha,\tau} + P_\ell^{\alpha,\tau} \right), \tag{4.26}$$

and the ℓth component of the vector $\mathbf{v}_i$ is

$$[\mathbf{v}_i]_\ell = \frac{1}{2}(-1)^{\frac{j}{2}} \binom{j}{\frac{j}{2}} u_i^0 + \sum_{s=1}^{\frac{j}{2}} (-1)^{\frac{j}{2}+s} \binom{j}{\frac{j}{2}+s} u_i^{s\ell}. \tag{4.27}$$

To avoid cluttered notations, we have suppressed dependence on j in the notation of vector $\mathbf{v}_i$. The above estimate shows that $\mathbf{T}_j^\alpha \cdot \mathbf{v}_i$ approximates the fractional Laplacian $(-\Delta_x)_j^{\frac{\alpha}{2}} f(x_i)$ at each given position x_i. Here, we assume that $u(r) = \mathcal{U}(x, r; f) \in C^{m,\nu}(\mathbb{R}^1)$ is an even function of r, or more precisely, $f(x) \in C^{m,\nu}(\mathbb{R}^n)$. Indeed, this additional assumption is only needed in the scheme (4.17), which is used to approximate the 1-D fractional Laplacian $\left(-\partial_r^2\right)_j^{\frac{\alpha}{2}}$ of (4.6).

Since the original fractional Laplacian (2.1) is a special case of the extended one (2.9) with $j = 2$ and $\alpha \in (0, 2)$, we have the following numerical formula for the fractional Laplacian (2.1):

$$(-\Delta_x)^{\frac{\alpha}{2}} f(x_i) \approx \mathbf{T}_2^\alpha \cdot \mathbf{v}_i = \frac{\omega_n}{4} C_{n,\alpha} \sum_{\ell=1}^{L} \left(\widetilde{P}_{\gamma,\ell}^{\alpha,\tau} + P_\ell^{\alpha,\tau} \right) \left(u_i^0 - u_i^\ell \right). \tag{4.28}$$

Moreover, when $j = 4$, we have

$$(-\Delta_x)_4^{\frac{\alpha}{2}} f(x_i) \approx \mathbf{T}_4^\alpha \cdot \mathbf{v}_i = \frac{\omega_n}{2} C_{n,\alpha,4} \sum_{\ell=1}^{L} \left(\widetilde{P}_{\gamma,\ell}^{\alpha,\tau} + P_\ell^{\alpha,\tau} \right) \left(3u_i^0 - 4u_i^\ell + u_i^{2\ell} \right). \tag{4.29}$$

If f is smooth enough and the spherical mean is computed to high-order accuracy, then the accuracy of the formula (4.29) will be higher than that of the formula (4.28).

Similarly, we also have a numerical method for applying the Riesz potential operator (2.5),

$$R_x^\alpha \varphi(x_i) \approx \frac{\omega_n}{2} C_{n,\alpha}^R \sum_{\ell=1}^{L} \left(\widetilde{P}_{\gamma,\ell}^{-\alpha,\tau} + P_\ell^{-\alpha,\tau} \right) u_i^\ell, \tag{4.30}$$

where $u_i^\ell \approx \mathcal{U}(x_i, r_\ell; \varphi)$.

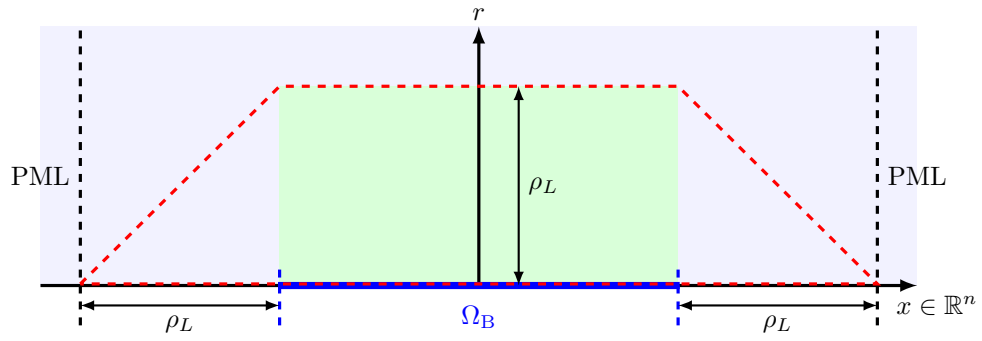

FIG. 1. *The truncation of the computational domain, the green area.*

4.5. Truncating the computational domain. We discuss how to truncate the computational domain when computing the spherical mean $\mathcal{U}(x, r; f)$. In Figure 1, the spatial axis for $x \in \mathbb{R}^n$ is shown by the horizontal axis, and the time-like variable $r \in [0, +\infty)$ is shown by the vertical axis. Thus, the entire space-time domain $(x, r) \in \mathbb{R}^n \times [0, +\infty)$ is the blue domain in this figure. The borderlines for imposing absorbing boundary conditions, such as PML, for this wave-like equation are indicated as the black dashed lines. The blue area between these two black dashed lines is the computational domain for the spherical mean $\mathcal{U}(x, r; f)$ in our method. Since the variable r is bounded by $\rho_L = L\tau$ according to the scheme (4.17), the "clean" enough numerical solution (or data) u_i^k of the spherical mean $\mathcal{U}(x, r; f)$ needed for computing the fractional Laplacian is located in the smaller area between the red dashed lines. Outside of this red dashed area, the data are polluted with errors from both the domain and the function f due to the PML boundary condition. In fact, each point x_i should be located inside the blue interval Ω_B on the x-axis so that the data u_i^k for the spherical mean $\mathcal{U}(x, r; f)$ are sampled in the green area $\Omega_B \times [0, \rho_L]$ in this figure.

4.6. The computational complexity of implementing Algorithm 1. Recall that the constant L is the truncation parameter for the r-direction, and, for the sake of simplicity, we assume that L^n is the total number of grid points $\{x_i\}$ over the blue domain Ω_B in the space $\mathbb{R}^n$. Thus, the total number of grid points $\{x_i\}$ is $(3L)^n$, i.e., $\mathcal{O}(L^n)$, in the spatial directions, and the number of data points u_i^k sampled in the domain $\mathbb{R}^n \times [0, \rho_L]$ is $\mathcal{O}(L^{n+1})$; see Figure 1.

The complexity of step (1A) in Algorithm 1 is $\mathcal{O}(L^{n+1})$, which consists of two components: costing $\mathcal{O}(L^{n+1})$ to solve the wave equation by a standard wave solver and costing $\mathcal{O}(L^{n+1})$ to carry out numerical integration of formula (3.14). Since the integrand of (3.14) is $(r^2 - t^2)^{\frac{n-3}{2}}$, the resulting numerical quadrature for n even is slightly different from that for n odd. When $n = 1$, the situation is trivial as shown in Darboux's equation (3.11); when $n > 1$ is odd, formula (3.14) can be numerically integrated with complexity $\mathcal{O}(L^{n+1})$ in a direct manner after expanding the integration weight into individual terms; and when n is even, formula (3.14) can be numerically integrated with complexity $\mathcal{O}(L^{n+1})$ in an indirect manner. For example, when $n = 2$, we use formula (3.19) to approximate formula (3.16), where the two constants of S and ϵ are chosen appropriately so that not only the errors from the two parts are balanced but the resulting numerical quadratures can be implemented efficiently as well; in our numerical examples, we have set $S = 2$, $\epsilon = \theta\tau$, and $\theta = 1$; thus, the

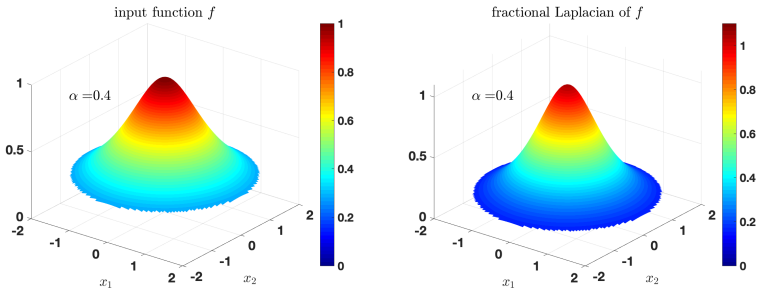

FIG. 2. *[Case 1, $\alpha = 0.4$]. Left: The input function f. Right: The fractional Laplacian of f.*

complexity of evaluating (3.19) is $\mathcal{O}(L^1)$ for computing all u_i^k $(k = 0, 1, \ldots, L)$ when x_i is fixed, and the resulting total complexity is $\mathcal{O}(L^{n+1})$. The same strategy as for $n = 2$ can be applied to other even n.

The complexity of step (1B) in Algorithm 1 is $\mathcal{O}(L^{n+1})$, which consists of two components: costing $\mathcal{O}(L^{n+1})$ to solve Darboux's (wave-like) equation directly by a standard wave solver and costing $\mathcal{O}(L^n)$ to compute the special initial condition (3.27) for small enough r.

It is easy to estimate the complexity of step (2) in Algorithm 1. Since applying the 1-D fractional Laplacian to u_i^k $(k = 0, 1, \ldots, L)$ at each grid point x_i boils down to computing a dot product of two vectors $\mathbf{T}_2^\alpha$ and $\mathbf{v}_i$ according to formula (4.25), the computational complexity is $\mathcal{O}(L^1)$ at each grid point x_i. Therefore, the overall complexity of step (2) is $\mathcal{O}(L^{n+1})$ in the computational domain.

Therefore, Algorithm 1 can be implemented efficiently with the overall complexity $\mathcal{O}(L^{n+1})$.

5. Computing actions of fractional Laplacians: Numerical examples. We present several examples to illustrate our numerical methods, in particular, the schemes (4.28) and (4.29) for computing actions of fractional Laplacians. These examples include smooth functions and functions with low regularities, and we also check the convergence rates for different cases. For the sake of simplicity, we work on the two-dimensional space only, $n = 2$. Unless otherwise stated, we use the formula (3.19) to generate spherical means.

5.1. Smooth case (Case 1). We first consider a smooth test function for our numerical scheme (4.28). For $x \in \mathbb{R}^n$, the input function f is given by

$$\text{Case 1:} \quad f(x) = \left(1 + |x|^2\right)^{-\frac{n-\alpha}{2}}, \tag{5.1}$$

and the fractional Laplacian of this smooth function f is also a smooth function in the entire space $\mathbb{R}^n$,

$$\text{Case 1:} \quad (-\Delta_x)^{\frac{\alpha}{2}} f(x) = \frac{2^\alpha \Gamma\left(\frac{n+\alpha}{2}\right)}{\Gamma\left(\frac{n-\alpha}{2}\right)} \left(1 + |x|^2\right)^{-\frac{n+\alpha}{2}}. \tag{5.2}$$

For $\alpha = 0.4$, as shown in Figure 2 (left), the graph of this test function (5.1) is a bell-shaped surface, and it decays to zero algebraically as $|x| \to \infty$, and the corresponding fractional Laplacian (5.2) has a smaller base since it decays faster than the original function (5.1); see Figure 2 (right).

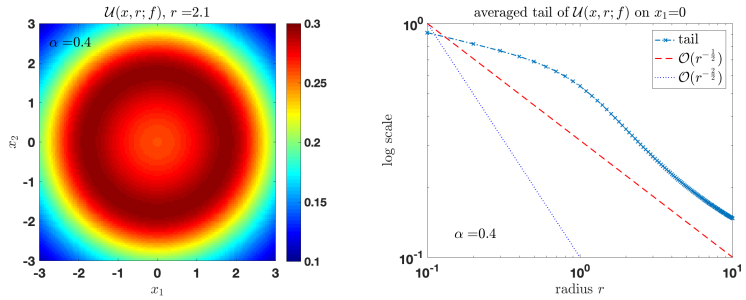

FIG. 3. *[Case 1, $\alpha = 0.4$]. Left: The spherical means $\mathcal{U}(x,r;f)$ at each grid point $x = (x_1, x_2)$ with $r = 2.1$. Right: The asymptotic behavior of the tail with $\beta = \frac{n-1}{2}$ for $n = 2$ (red dashed) or 3 (blue dotted).*

TABLE 1

The computational complexity and CPU time (s: second) for evaluating u_i^k, $k = 1, 2, \ldots, L$ for $n = 2$.

Truncation parameter L	Complexity of (3.27) $\mathcal{O}(L^{2+1})$	Complexity of (3.19) $\mathcal{O}(L^{2+1})$	Complexity of (3.16) $\mathcal{O}(L^{2+2})$
128	0.19 s	0.19 s	0.94 s
256	0.69 s	0.65 s	8.47 s
512	3.46 s	3.62 s	129.91 s
1024	32.98 s	33.45 s	1849.79 s
2048	235.81 s	243.90 s	37510.42 s

According to our numerical method, given f, the goal of step (1A) or (1B) in our algorithm is to generate the spherical mean $\mathcal{U}(x,r;f)$ as defined in (3.1). By utilizing the numerical schemes that we have developed, we can calculate the spherical mean numerically, u_i^k of radius r_k at each grid point $(x_1, x_2)_i$ in $\mathbb{R}^2$; see Figure 3 (left) for $r_k = 2.1$. Meanwhile, we also check the asymptotic behavior of the function $\mathcal{U}(x,r;f)$ with respect to the variable r to estimate the order β of r in (3.34). As shown in Figure 3 (right), the blue dash-dot line with cross markers "$\times$" is the averaged tail of $\mathcal{U}(x,r;f)$ on $x_1 = 0$, and the order β is close to $\frac{1}{2}$ (the red dashed line), which verifies the estimated order $\frac{n-1}{2}$ when $n = 2$. Consequently, this order estimate justifies the truncated tail estimate (4.16) for the 1-D fractional Laplacian.

Moreover, we also check the computational complexity of generating spherical means, which is crucial for the success of our method. The comparison of complexities of the three approaches (3.16), (3.19), and (3.27) is shown in Table 1, in which the spherical means u_i^k are evaluated for all $k = 0, 1, \ldots, L$ and i in the computational domain.

Now we discuss step (2) in Algorithm 1. Starting from the spherical means $\mathcal{U}(x,r;f)$, we compute the fractional Laplacian of the given function f by applying the 1-D fractional Laplacian to $\mathcal{U}(x,r;f)$. After we compute the vector $\mathbf{T}_2^\alpha$ and the vector $\mathbf{v}_i$, we apply the scheme (4.28), and the result at the grid points $(x_1, x_2)_i$ is presented in Figure 4. The left panel of Figure 4 shows a bell-shaped surface inside the unit ball, which approximates quite well the exact function (5.2) shown in Figure 2 (right). The comparison between these two functions on the line $x_1 = 0$ is shown on the right panel of Figure 4, where the red dot-dashed line is the exact function (5.2) (fracLap) and the blue line is our numerical result (output). This example shows that our numerical method obtains good results for computing the action of the fractional Laplacian when the input function f is smooth enough.

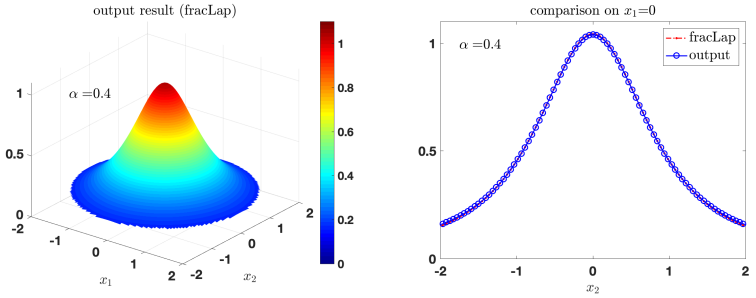

FIG. 4. *[Case 1, $\alpha = 0.4$]. Left: The output result. Right: The comparison between the exact and computed fractional Laplacian on the line $x_1 = 0$.*

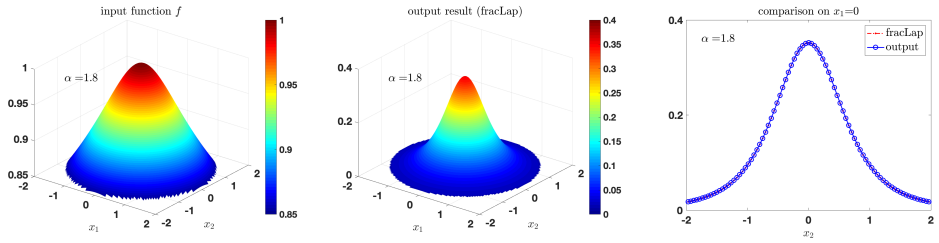

FIG. 5. *[Case 1, $\alpha = 1.8$]. Left: The input function f. Middle: The output result. Right: The comparison between the exact and computed fractional Laplacian on the line $x_1 = 0$.*

Even for a larger parameter, $\alpha = 1.8$, our numerical method is still able to compute an accurate approximation, as shown in Figure 5; this is in sharp contrast to the behavior of the numerical method in [23] in the sense that the numerical accuracy of the method in [23] deteriorates as α goes to 2.

5.2. Functions in $C^{1,\frac{\alpha}{2}}(\mathbb{R}^n)$ (Case 2). We consider a test function which has a lower regularity and is Hölder continuous only. It is in the space $C^{1,\frac{\alpha}{2}}(\mathbb{R}^n)$, taking the form

$$\text{Case 2(a):} \quad f(x) = \left(1 - |x|^2\right)^{1+\frac{\alpha}{2}}, \quad |x| < 1, \tag{5.3}$$

and vanishing outside the unit ball in $\mathbb{R}^n$: $f(x) \equiv 0$ for $|x| \geqslant 1$. We denote this piecewise continuous function as $f(x) = \left(1 - |x|^2\right)_+^{1+\frac{\alpha}{2}}$, where the notation $(\cdot)_+$ indicates that $(y)_+ = y$ if $y > 0$ and $(y)_+ = 0$ if $y \leqslant 0$. For this hat function f, Dyda [17] and Samko [40] obtained the following formula for the fractional Laplacian:

$$\text{Case 2(a):} \quad (-\Delta_x)^{\frac{\alpha}{2}} f(x) = \frac{2^\alpha \Gamma\left(\frac{\alpha}{2}+2\right)\Gamma\left(\frac{n+\alpha}{2}\right)}{\Gamma\left(\frac{n}{2}\right)}\left(1 - \left(1+\frac{\alpha}{n}\right)|x|^2\right), \quad |x| < 1. \tag{5.4}$$

The numerical results are shown in Figure 6 for $\alpha = 0.4$ and in Figure 7 for $\alpha = 1.8$ respectively. These results are similar to those of Case 1 in the last subsection. In both cases, our numerical method can capture the main structure of the fractional Laplacian of the given input function f. However, there are slight mismatches on the boundary of the unit ball for $\alpha = 1.8$ since the input test function f has lower regularity on the boundary $|x| = 1$.

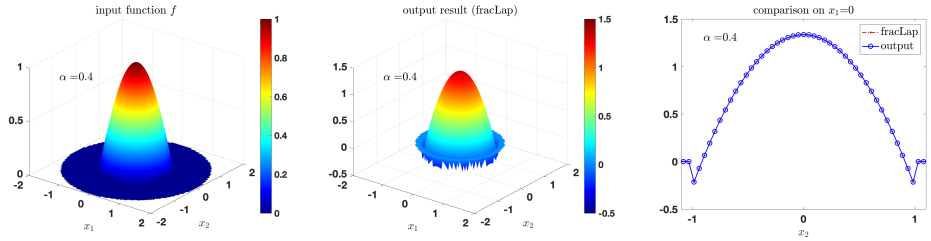

FIG. 6. *[Case* 2(a), $\alpha = 0.4$*]. Left: The input function f. Middle: The output result. Right: The comparison between the exact and computed fractional Laplacian on the line $x_1 = 0$.*

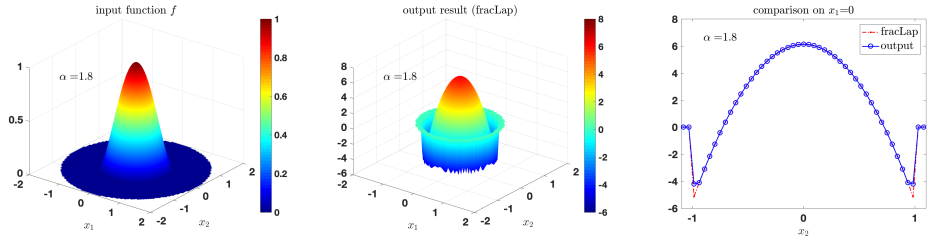

FIG. 7. *[Case* 2(a), $\alpha = 1.8$*]. Left: The input function f. Middle: The output result. Right: The comparison between the exact and computed fractional Laplacian on the line $x_1 = 0$.*

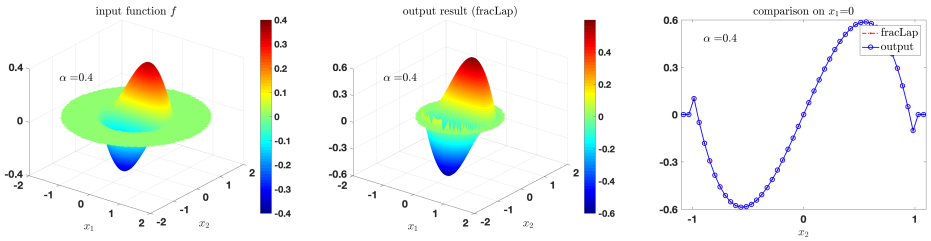

FIG. 8. *[Case* 2(b), $\alpha = 0.4$*]. Left: The input function f. Middle: The output result. Right: The comparison between the exact and computed fractional Laplacian on the line $x_1 = 0$.*

We modify the test example in Case 2(a) slightly to show robustness of our numerical method. The modified test function is

$$\text{Case 2(b):} \quad f(x) = \left(1 - |x|^2\right)_+^{1+\frac{\alpha}{2}} x_2, \tag{5.5}$$

and the corresponding fractional Laplacian is

$$\begin{aligned} &\text{Case 2(b):} \, (-\Delta_x)^{\frac{\alpha}{2}} f(x) \\ &= \frac{2^\alpha \Gamma\left(\frac{\alpha}{2}+2\right)\Gamma\left(\frac{n+\alpha}{2}+1\right)}{\Gamma\left(\frac{n}{2}+1\right)} \left(1 - \left(1 + \frac{\alpha}{n+2}\right)|x|^2\right) x_2, \quad |x| < 1. \end{aligned} \tag{5.6}$$

Figure 8 and Figure 9 show the results for $\alpha = 0.4$ and $\alpha = 1.8$, respectively.

5.3. Convergence rates. Now, according to the error estimate (4.25), we show convergence rates measured in terms of the following uniform errors:

$$\max_{\forall i:|x_i|<1} \left| (-\Delta_x)_j^{\frac{\alpha}{2}} f(x_i) - \mathbf{T}_j^\alpha \cdot \mathbf{v}_i \right|. \tag{5.7}$$

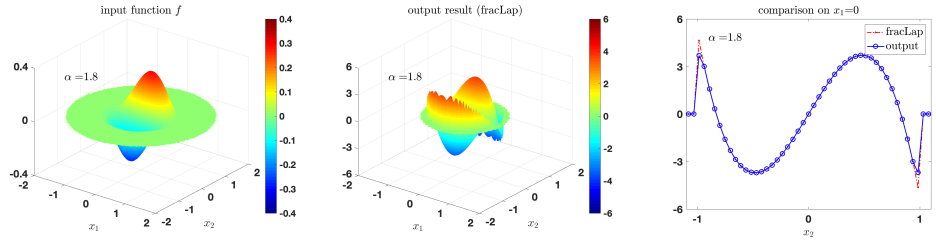

FIG. 9. *[Case* 2(b), $\alpha = 1.8$*]. Left: The input function* f*. Middle: The output result. Right: The comparison between the exact and computed fractional Laplacian on the line* $x_1 = 0$*.*

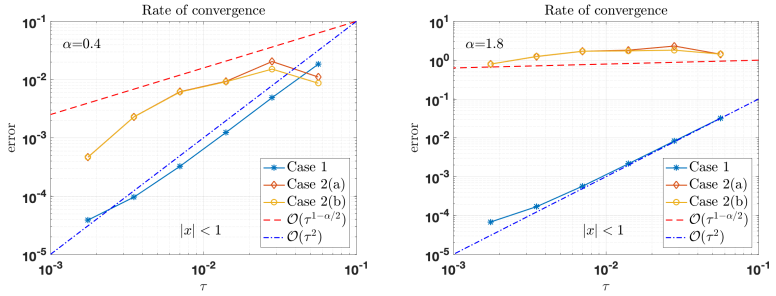

FIG. 10. *Rate of convergence,* $|x| < 1$*. Left:* $\alpha = 0.4$*. Right:* $\alpha = 1.8$*.*

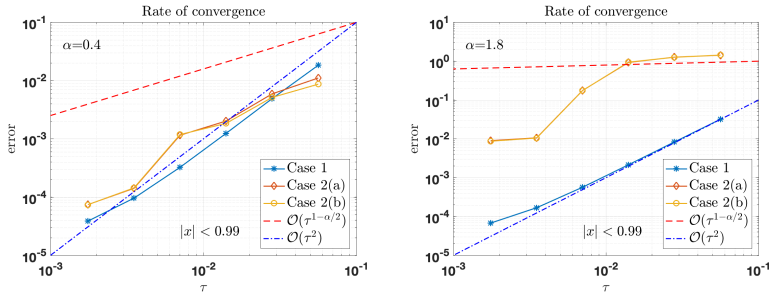

FIG. 11. *Rate of convergence in the regular part,* $|x| < 0.99$*. Left:* $\alpha = 0.4$*. Right:* $\alpha = 1.8$*.*

The convergence rates in different settings are shown in Figures 10–12 with a log-log scale. The red dashed line shown on each subfigure is the theoretical convergence rate for functions in Hölder space $C^{m,\nu}(\mathbb{R}^n)$ so that the expected error is $\mathcal{O}(\tau^{m+\nu-\alpha})$, where τ is the step size in the radial direction. Meanwhile, the blue dash-dot line is the theoretical convergence rate for generating spherical means of a given function, i.e., $\mathcal{O}(\tau^2)$. The numerical convergence rates for the smooth test function (5.1) in Case 1 are marked by blue "$*$," and the rates for the test functions (5.3) and (5.5) in Case 2 are marked by red "$\circ$" and orange "$\diamondsuit$," respectively.

When $\alpha = 0.4$, the left panel of Figure 10 demonstrates the following convergence rates: For the smooth function in Case 1, the convergence rate is almost $\mathcal{O}(\tau^2)$; for the test functions in Hölder space $C^{m,\nu}(\mathbb{R}^n) = C^{1,\frac{\alpha}{2}}(\mathbb{R}^n)$, the rate is close to the theoretical one, $1 - \frac{\alpha}{2} = 0.8$. When $\alpha = 1.8$, the right panel of Figure 10 demonstrates the convergence rates which are similar to those when $\alpha = 0.4$: For the

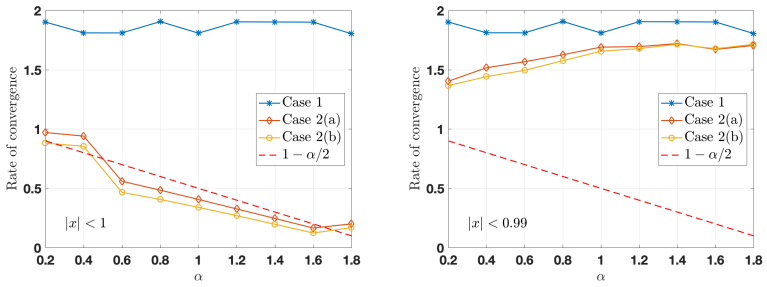

FIG. 12. *Rate of convergence with respect to* $\alpha \in (0,2)$. *Left:* $|x|<1$. *Right:* $|x|<0.99$.

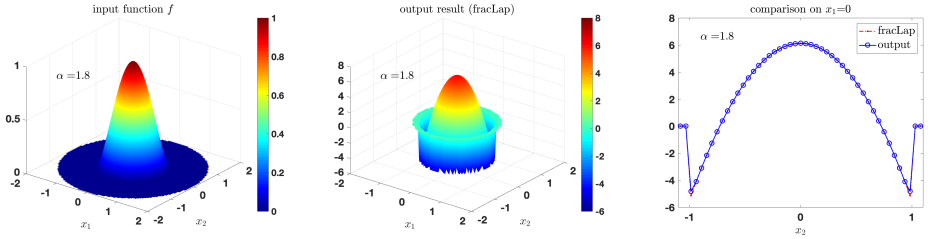

FIG. 13. *[Case* 2(a), $\alpha = 1.8$, *extended]. Left: The input function* f. *Middle: The output result. Right: The comparison between the exact and computed extended fractional Laplacian on a line* $x_1 = 0$.

smooth function in Case 1, the convergence rate is still close to $\mathcal{O}(\tau^2)$; for the test functions in Hölder space $C^{m,\nu}(\mathbb{R}^n) = C^{1,\frac{\alpha}{2}}(\mathbb{R}^n)$, the rate is close to the theoretical one, $1-\frac{\alpha}{2} = 0.1$.

The above convergence results indicate that the convergence rate deteriorates as the regularity of test functions decreases. However, if we only consider the regular part of the test functions in Case 2, that is, $|x| < 0.99$, we still can obtain an order of convergence which is similar to the one in Case 1 since the misfit related to the irregular part is close to the boundary $|x| = 1$; see Figure 11 for $\alpha = 0.4$ (left) and $\alpha = 1.8$ (right), respectively.

Figure 12 shows the uniform convergence rates for α varying in the interval $(0,2)$. When the functions are sufficiently smooth such as those in Case 1, the convergence rate is roughly $\mathcal{O}(\tau^2)$; when the function is of low regularity, such as the one in Case 2 which is in the Hölder space $C^{1,\frac{\alpha}{2}}(\mathbb{R}^n)$, the rate is close to its theoretical order $1-\frac{\alpha}{2}$; see Figure 12 (left). Meanwhile, if we only consider the uniform errors in the regular part, $|x| < 0.99$, the convergence rates of the two numerical fractional Laplacians in Case 2 are greater than 1.3; see Figure 12 (right).

6. Computing actions of extended fractional Laplacians: Numerical examples. We also test our numerical scheme (4.29) to compute the extended fractional Laplacian. We take $n = 2$. Here we use the formula (3.19) to generate spherical means. We choose the test functions to be (5.3) in Case 2(a) and (5.5) in Case 2(b), respectively. The numerical results in Figures 13 and 14 with $\alpha = 1.8$ demonstrate that the extended numerical fractional Laplacian reduces the misfits on the boundary of the unit ball, which can be seen by comparing Figure 7 (right) with Figure 13 (right) and Figure 9 (right) with Figure 14 (right).

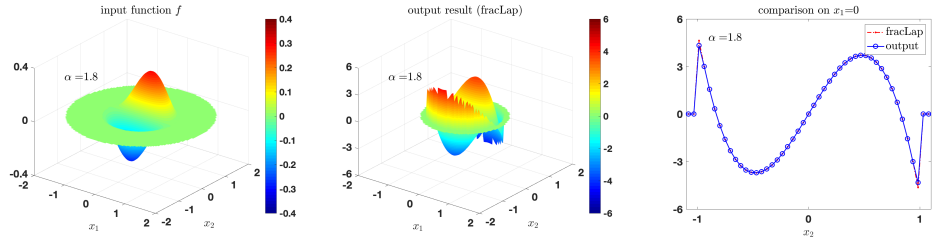

FIG. 14. *[Case* 2(b), $\alpha = 1.8$, *extended]. Left: The input function* f. *Middle: The output result. Right: The comparison between the exact and computed extended fractional Laplacian on a line* $x_1 = 0$.

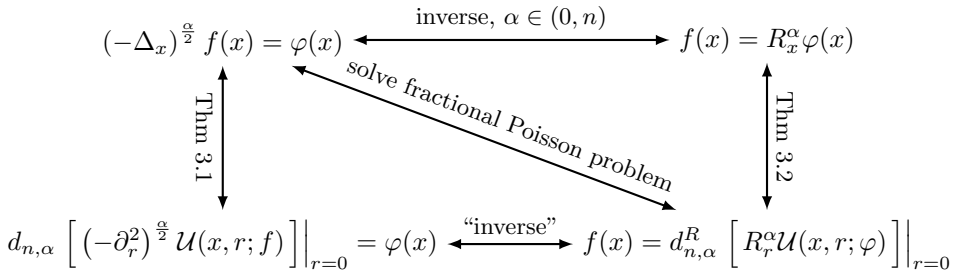

FIG. 15. *The relationship between the Riesz derivative operator* $\left(-\partial_r^2\right)^{\frac{\alpha}{2}}$ *and the Riesz potential operator* R_r^α *with respect to* $r \in \mathbb{R}^1$.

7. Applying Riesz potential operators to solve fractional Poisson equations: Examples. To compute the action of the Riesz potential operator, we use the formula (3.19) to generate spherical means. We take $n = 2$. Consider the following fractional Poisson equation in the entire space,

$$(-\Delta_x)^{\frac{\alpha}{2}} f(x) = \varphi(x), \quad x \in \mathbb{R}^n, \tag{7.1}$$

where both φ and f are in suitable function spaces, the right-hand-side function $\varphi(x)$ is given, and $f(x)$ is the unknown function. Recall that when $\alpha \in (0, n)$, the Riesz derivative operator (i.e., the fractional Laplace operator $(-\Delta_x)^{\frac{\alpha}{2}}$) is an inverse operator to the Riesz potential operator R_x^α with respect to $x \in \mathbb{R}^n$; see [41, page 512]. Consequently, we have the formula

$$f(x) = R_x^\alpha \varphi(x), \quad x \in \mathbb{R}^n, \tag{7.2}$$

which yields a solution to the fractional Poisson equation (7.1). Furthermore, by using Theorems 3.1 and 3.2, we can obtain that the Riesz derivative operator $\left(-\partial_r^2\right)^{\frac{\alpha}{2}}$ is also an inverse operator to the Riesz potential operator R_r^α with respect to $r \in \mathbb{R}^1$; see Figure 15. Therefore, we can solve the fractional Poisson problem (7.1) directly by applying the numerical scheme (4.30) of the Riesz potential operator.

Now we consider the extended Dirichlet problem (1.2). For convenience, we restate the problem as the following: Find $f : \Omega \to \mathbb{R}$ satisfying

$$(-\Delta_x)^{\frac{\alpha}{2}} \widetilde{f} = \varphi \quad \text{in } \Omega, \qquad \widetilde{f} = 0 \quad \text{in } \Omega^c = \mathbb{R}^n \backslash \Omega, \tag{7.3}$$

where $\varphi : \Omega \to \mathbb{R}$ is a given function in a suitable space and $\widetilde{w}$ is the extension by zero to $\mathbb{R}^n$ of a function $w : \Omega \to \mathbb{R}$.

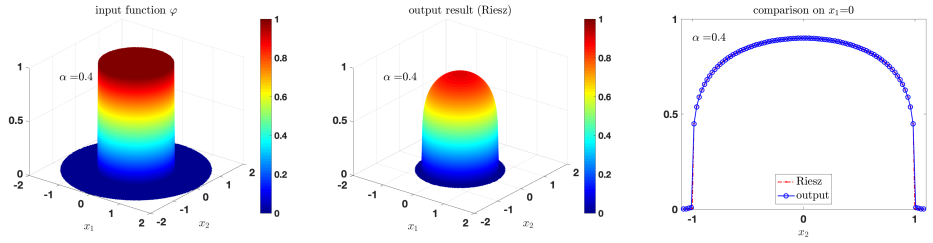

FIG. 16. *[Riesz* (a), $\alpha = 0.4$*]. Left: The right-hand-side (input for the Riesz potential operator)* φ*. Middle: The numerical solution (output from the Riesz potential operator)* f*. Right: The comparison between the exact and numerical solution on the line* $x_1 = 0$*.*

To apply the Riesz potential operator to solve the extended Dirichlet problem (7.3), we first extend the given function φ by zero to $\mathbb{R}^n$ to obtain $\widetilde{\varphi}$, and then we apply the operator to $\widetilde{\varphi}$, yielding

$$\bar{f}(x) = \left[R_x^\alpha \widetilde{\varphi}\right](x) \approx \widetilde{f}(x) \qquad \Rightarrow \qquad \bar{f}(x)\Big|_{x\in\Omega} = \left[R_x^\alpha \widetilde{\varphi}\right](x)\Big|_{x\in\Omega} \approx \widetilde{f}(x)\Big|_{x\in\Omega}, \tag{7.4}$$

where $\bar{f}(x)|_{x\in\Omega}$ gives an approximation to $f(x) : x \in \Omega \to \mathbb{R}$. Although we have not established the convergence theory for this approach of solving the extended Dirichlet problem, the following numerical examples indicate that this is a feasible method.

Riesz (a). We choose the right-hand side of the fractional Poisson equation (7.1) to be

$$\varphi(x) = 1 \quad \text{for} \quad |x| < 1 \tag{7.5}$$

so that the corresponding exact solution f is in the Hölder space $C^{0,\frac{\alpha}{2}}(\mathbb{R}^n)$ and takes the following form:

$$f(x) = \frac{\Gamma\left(\frac{n}{2}\right)}{2^\alpha \Gamma\left(\frac{\alpha}{2}+1\right)\Gamma\left(\frac{n+\alpha}{2}\right)} \left(1-|x|^2\right)_+^{\frac{\alpha}{2}}; \tag{7.6}$$

in fact, φ is the fractional Laplacian of the function f, and it is constant inside the unit ball.

Take $\alpha = 0.4$. Figure 16 shows the right-hand-side (input) function φ in the left panel and the corresponding numerical solution (output) f in the middle panel. The comparison between the exact and numerical solution on the line $x_1 = 0$ is shown in the right panel of Figure 16, where the red dot-dashed line indicates the exact solution (7.6) and the blue line indicates our numerical solution; the two solutions match each other very well.

Riesz (b). We choose the right-hand side of the fractional Poisson equation (7.1) to be

$$\varphi(x) = x_2 \quad \text{for} \quad |x| < 1 \tag{7.7}$$

so that the exact solution is also in the Hölder space $C^{0,\frac{\alpha}{2}}(\mathbb{R}^n)$ and takes the following form:

$$f(x) = \frac{\Gamma\left(\frac{n}{2}+1\right)}{2^\alpha \Gamma\left(\frac{\alpha}{2}+1\right)\Gamma\left(\frac{n+\alpha}{2}+1\right)} \left(1-|x|^2\right)_+^{\frac{\alpha}{2}} x_2. \tag{7.8}$$

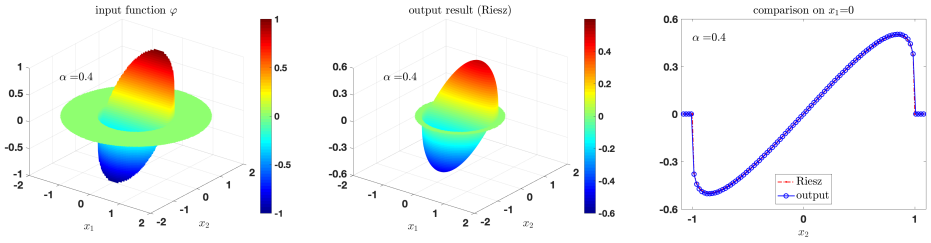

FIG. 17. *[Riesz* (b), $\alpha = 0.4$*]. Left: The right-hand-side (input for the Riesz potential operator)* φ*. Middle: The numerical solution (output from the Riesz potential operator)* f*. Right: The comparison between the exact and numerical solution on the line* $x_1 = 0$*.*

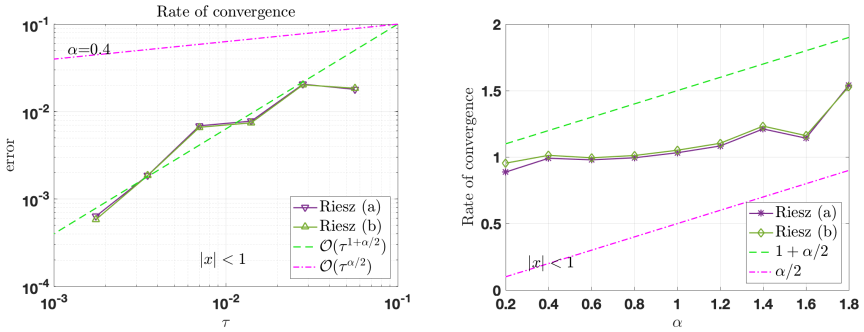

FIG. 18. *[Riesz case]. Left: Rate of convergence when* $|x| < 1$ *and* $\alpha = 0.4$*. Right: Rate of convergence with respect to* $\alpha \in (0, 2)$*.*

Take $\alpha = 0.4$. Figure 17 (left) shows the right-hand-side function φ (7.7), which is a linear function of x_2 inside the unit ball, and Figure 17 (middle) shows the corresponding numerical solution f. The comparison in Figure 17 (right) shows that the numerical (output) result matches with the exact (Riesz) solution (7.8) quite well inside the unit ball.

Next, we numerically study convergence of applying the Riesz potential operator to solve the fractional Poisson problem (7.1). Here the right-hand-side function φ is chosen to be (7.5) in Riesz (a) and (7.7) in Riesz (b), marked by purple "$\triangledown$" and green "$\triangle$" in Figure 18, respectively. Figure 18 (left) shows the order of convergence rates in terms of mesh sizes for $\alpha = 0.4$. Figure 18 (right) demonstrates that the order of uniform convergence rates is close to 1 for varying α in $(0, 2)$.

8. Conclusion. We propose a novel numerical method for computing multidimensional fractional Laplacians via spherical means. Our numerical tests indicate that our method based on interpolations or weighted trapezoidal rules computes fractional Laplacians of sufficiently smooth functions with second-order accuracy and those of functions in $C^{m,\nu}(\mathbb{R}^n)$ with theoretical accuracy order $m + \nu - \alpha$. Moreover, our method can be also applied to solve the fractional Poisson problem or the homogeneous extended Dirichlet problem. Treating the anomalous diffusion problem and the obstacle problem involving fractional Laplacians are ongoing projects.

Acknowledgment. Qian would like to thank Dr. Robert Burridge for discussions on solving Darboux's differential equation. Qian would like to dedicate this paper to Professor Jiaqi Liu on the occasion of his 80th birthday!

REFERENCES

[1] G. Acosta, F. M. Bersetche, and J. P. Borthagaray, *A short FE implementation for a 2d homogeneous Dirichlet problem of a fractional Laplacian*, Comput. Math. Appl., 74 (2017), pp. 784–816.

[2] G. Acosta and J. P. Borthagaray, *A fractional Laplace equation: Regularity of solutions and finite element approximations*, SIAM J. Numer. Anal., 55 (2017), pp. 472–495.

[3] G. Acosta, J. P. Borthagaray, O. Bruno, and M. Maas, *Regularity theory and high order numerical methods for the (1D)-fractional Laplacian*, Math. Comp., 87 (2018), pp. 1821–1857.

[4] L. Banjai, J. Melenk, R. Nochetto, E. Otarola, A. Salgado, and C. Schwab, *Tensor FEM for spectral fractional diffusion*, Found. Comput. Math., 19 (2019), pp. 901–962.

[5] J. Bertoin, *Lévy Processes*, Cambridge Tracts in Math. 121, Cambridge University Press, Cambridge, 1996.

[6] A. Bonito, J. P. Borthagaray, R. H. Nochetto, E. Otárola, and A. J. Salgado, *Numerical methods for fractional diffusion*, Comput. Vis. Sci., (2018), doi:10.1007/s00791-018-0289-y.

[7] A. Bonito, W. Lei, and J. E. Pasciak, *Numerical approximation of the integral fractional Laplacian*, Numer. Math., 142 (2019), pp. 235–278.

[8] X. Cabré and J. Tan, *Positive solutions of nonlinear problems involving the square root of the Laplacian*, Adv. Math., 224 (2010), pp. 2052–2093.

[9] L. Caffarelli and L. Silvestre, *An extension problem related to the fractional Laplacian*, Comm. Partial Differential Equations, 32 (2007), pp. 1245–1260.

[10] L. A. Caffarelli and P. R. Stinga, *Fractional elliptic equations, Caccioppoli estimates and regularity*, Ann. Inst. H. Poincaré Anal. Non Linéaire, 33 (2016), pp. 767–807.

[11] L. Chen, R. H. Nochetto, E. Otárola, and A. J. Salgado, *A PDE approach to fractional diffusion: A posteriori error analysis*, J. Comput. Phys., 293 (2015), pp. 339–358.

[12] L. Chen, R. H. Nochetto, E. Otárola, and A. J. Salgado, *Multilevel methods for nonuniformly elliptic operators and fractional diffusion*, Math. Comp., 85 (2016), pp. 2583–2607.

[13] S. Chen and J. Shen, *An efficient and accurate numerical method for the spectral fractional Laplacian equation*, J. Sci. Comput., 82 (2020), pp. 1–25.

[14] R. Courant and D. Hilbert, *Methods of Mathematical Physics*, Vol. 2, Interscience Publishers, New York, 1962.

[15] M. D'Elia and M. Gunzburger, *The fractional Laplacian operator on bounded domains as a special case of the nonlocal diffusion operator*, Comput. Math. Appl., 66 (2013), pp. 1245–1260.

[16] S. Duo, H. W. van Wyk, and Y. Zhang, *A novel and accurate finite difference method for the fractional Laplacian and the fractional Poisson problem*, J. Comput. Phys., 355 (2018), pp. 233–252.

[17] B. Dyda, *Fractional calculus for power functions and eigenvalues of the fractional Laplacian*, Fract. Calc. Appl. Anal., 15 (2012), pp. 536–555.

[18] M. Felsinger, M. Kassmann, and P. Voigt, *The Dirichlet problem for nonlocal operators*, Math. Z., 279 (2015), pp. 779–809.

[19] T. Gao, J. Duan, X. Li, and R. Song, *Mean exit time and escape probability for dynamical systems driven by Lévy noises*, SIAM J. Sci. Comput., 36 (2014), pp. A887–A906.

[20] T. Görner, R. Hielscher, and S. Kunis, *Efficient and accurate computation of spherical mean values at scattered center points*, Inverse Probl. Imaging, 6 (2012), pp. 645–661.

[21] Y. Hu, C. Li, and H. Li, *The finite difference method for Caputo-type parabolic equation with fractional Laplacian: One-dimension case*, Chaos Solitons Fractals, 102 (2017), pp. 319–326.

[22] Y. Hu, C. Li, and H. Li, *The finite difference method for Caputo-type parabolic equation with fractional Laplacian: More than one space dimension*, Int. J. Comput. Math., 95 (2018), pp. 1114–1130.

[23] Y. Huang and A. Oberman, *Numerical methods for the fractional Laplacian: A finite difference-quadrature approach*, SIAM J. Numer. Anal., 52 (2014), pp. 3056–3084.

[24] Y. Huang and A. Oberman, *Finite Difference Methods for Fractional Laplacians*, https://arxiv.org/abs/1611.00164, 2016.

[25] F. John, *Plane Waves and Spherical Means: Applied to Partial Differential Equations*, Interscience Publishers, New York, 1955.

[26] J. Keiner, S. Kunis, and D. Potts, *Using NFFT 3—A software library for various nonequispaced fast Fourier transforms*, ACM Trans. Math. Softw., 36 (2009), pp. 19:1–19:30.

[27] S. Kovač, J. Pečarić, and A. Perušić, *Estimations of the difference between two weighted integral means and application of the Steffensen's inequality*, An. Univ. Craiova Mat. Comp. Sci. Ser., 43 (2016), pp. 128–140.
[28] S. Kunis and I. Melzer, *A stable and accurate butterfly sparse Fourier transform*, SIAM J. Numer. Anal., 50 (2012), pp. 1777–1800.
[29] M. Kwaśnicki, *Ten equivalent definitions of the fractional Laplace operator*, Fract. Calc. Appl. Anal., 20 (2017), pp. 7–51.
[30] A. Lischke, G. Pang, M. Gulian, F. Song, C. Glusa, X. Zheng, Z. Mao, W. Cai, M. M. Meerschaert, M. Ainsworth, and G. E. Karniadakis, *What Is the Fractional Laplacian?*, preprint, https://arxiv.org/abs/1801.09767 [math.NA], 2018.
[31] B. B. Mandelbrot, *The Fractal Geometry of Nature*, W. H. Freeman, San Francisco, 1982.
[32] R. Metzler and J. Klafter, *The random walk's guide to anomalous diffusion: A fractional dynamics approach*, Phys. Rep., 339 (2000), pp. 1–77.
[33] R. Metzler and J. Klafter, *The Restaurant at the end of the random walk: Recent developments in the description of anomalous transport by fractional dynamics*, J. Phys. A, 37 (2004), pp. R161–R208.
[34] V. Minden and L. Ying, *A Simple Solver for the Fractional Laplacian in Multiple Dimensions*, preprint, https://arxiv.org/abs/1802.03770 [math.NA], 2018.
[35] R. Musina and A. I. Nazarov, *On fractional Laplacians*, Comm. Partial Differential Equations, 39 (2014), pp. 1780–1790.
[36] R. H. Nochetto, E. Otárola, and A. J. Salgado, *A PDE approach to fractional diffusion in general domains: A priori error analysis*, Found. Comput. Math., 15 (2015), pp. 733–791.
[37] C. Pozrikidis, *The Fractional Laplacian*, CRC Press, Boca Raton, FL, 2016.
[38] X. Ros-Oton, *Nonlocal elliptic equations in bounded domains: A survey*, Publ. Mat., 60 (2016), pp. 3–26.
[39] A. I. Saichev and G. M. Zaslavsky, *Fractional kinetic equations: Solutions and applications*, Chaos, 7 (1997), pp. 753–764.
[40] S. G. Samko, *Hypersingular Integrals and Their Applications*, Analytical Methods and Special Functions 5, CRC Press, Boca Raton, FL, 2002.
[41] S. G. Samko, A. A. Kilbas, and O. I. Marichev, *Fractional Integrals and Derivatives: Theory and Applications*, Gordon and Breach, Yverdon, Switzerland, 1993.
[42] R. Servadei and E. Valdinoci, *On the spectrum of two different fractional operators*, Proc. Roy. Soc. Edinburgh Sect. A, 144 (2014), pp. 831–855.
[43] I. M. Sokolov and J. Klafter, *From diffusion to anomalous diffusion: A century after Einstein's Brownian motion*, Chaos, 15 (2005), 026103.
[44] P. R. Stinga and J. L. Torrea, *Extension problem and Harnack's inequality for some fractional operators*, Comm. Partial Differential Equations, 35 (2010), pp. 2092–2122.
[45] X. Tian and Q. Du, *Analysis and comparison of different approximations to nonlocal diffusion and linear peridynamic equations*, SIAM J. Numer. Anal., 51 (2013), pp. 3458–3482.
[46] E. Valdinoci, *From the long jump random walk to the fractional Laplacian*, Boll. Soc. Española Mat. Apl. (2009), pp. 33–44.
[47] J. L. Vázquez, *The mathematical theories of diffusion: Nonlinear and fractional diffusion*, in Nonlocal and Nonlinear Diffusions and Interactions: New Methods and Directions, Lecture Notes in Math. 2186, Springer, New York, 2017, pp. 205–278.
[48] L. Ying, *Sparse Fourier transform via butterfly algorithm*, SIAM J. Sci. Comput., 31 (2009), pp. 1678–1694.